IMMUNOLOGY

Piezo1 channels restrain regulatory T cells but are dispensable for effector CD4$^+$ T cell responses

Amit Jairaman[1†], Shivashankar Othy[1†], Joseph L. Dynes[1], Andriy V. Yeromin[1], Angel Zavala[1], Milton L. Greenberg[1], Jamison L. Nourse[1,2], Jesse R. Holt[1,2], Stuart M. Cahalan[3,4], Francesco Marangoni[1], Ian Parker[1,5], Medha M. Pathak[1,2,6,7], Michael D. Cahalan[1,8]*

T lymphocytes encounter complex mechanical cues during an immune response. The mechanosensitive ion channel, Piezo1, drives inflammatory responses to bacterial infections, wound healing, and cancer; however, its role in helper T cell function remains unclear. In an animal model for multiple sclerosis, experimental autoimmune encephalomyelitis (EAE), we found that mice with genetic deletion of Piezo1 in T cells showed diminished disease severity. Unexpectedly, Piezo1 was not essential for lymph node homing, interstitial motility, Ca^{2+} signaling, T cell proliferation, or differentiation into proinflammatory T helper 1 (T_H1) and T_H17 subsets. However, Piezo1 deletion in T cells resulted in enhanced transforming growth factor–β (TGFβ) signaling and an expanded pool of regulatory T (T_{reg}) cells. Moreover, mice with deletion of Piezo1 specifically in T_{reg} cells showed significant attenuation of EAE. Our results indicate that Piezo1 selectively restrains T_{reg} cells, without influencing activation events or effector T cell functions.

INTRODUCTION

CD4$^+$ helper T lymphocytes orchestrate adaptive immune responses through their exquisite ability to discriminate antigens presented on antigen presenting cells (APCs) and to proliferate and differentiate into effector subsets that transmigrate and home to target tissues. During an immune response, T cells experience complex mechanical cues as they actively probe the surface of APCs, navigate barriers, squeeze through tight interstitial spaces, and execute their antigen search strategies in tissues of varied architecture (*1*) while also actively generating internal forces through cytoskeletal reorganization and membrane tension (*2*–*4*). Molecular mechanisms by which T cells sense mechanical forces and integrate mechanosignaling with biochemical pathways downstream of T cell receptor (TCR) activation are not well understood. Recent studies have focused on the TCR itself as a mechanosensor that regulates signaling through formation of TCR–peptide major histocompatibility complex catch bonds in response to tensile forces and whose activity is regulated by cytoskeletal rearrangements and stiffness of local environment (*2*, *5*–*7*). Additional mechanisms of mechanotransduction, mediated in particular by mechanically activated ion channels, could act in concert with or independently of TCR signaling to shape both effector and regulatory T (T_{reg}) cell function. However, the role of mechanosensitive ion channels in CD4$^+$ T cell function remains relatively unexplored.

Piezo1 constitutes the pore-forming subunit of trimeric nonselective cationic channels that are broadly expressed in mammalian cells and are activated by a variety of mechanical stimuli including shear stress, osmotic swelling, cyclical pressure, and traction forces (*8*–*10*). Piezo1 channels are permeable to Ca^{2+} ions and contribute to Ca^{2+} signaling, cell migration, and gene transcription at the cellular level and consequently regulate vital physiological functions including red blood cell (RBC) volume, blood pressure, vascular development, bone formation, and differentiation of neural stem cells (*11*–*16*). Mutations in Piezo1 have also been associated with hereditary xerocytosis, congenital lymphatic dysplasia, changes in iron metabolism, and resistance to malaria in human individuals (*17*–*20*). Recent studies have highlighted a potential role for Piezo1 in the innate immune system. In macrophages, Piezo1 channel activity alters gene expression and phagocytic activity and polarizes cells toward proinflammatory responses (*20*, *21*). In monocytes, Piezo1 channels sense cyclical mechanical forces in the lung and are required to mount proinflammatory responses in a mouse model of *Pseudomonas* infection (*22*). Expression of Piezo1 is also associated with expansion of myeloid-derived suppressor cells, leading to tumor progression in a mouse cancer model (*23*). These studies raise intriguing questions about the regulatory role of Piezo1 in normal adaptive immune functions and in autoimmunity.

In this study, we evaluated the role of Piezo1 in CD4$^+$ helper T cell function in a murine model of experimental autoimmune encephalomyelitis (EAE). Induction and progression of EAE depends on several aspects of CD4$^+$ T cell biology including the initial steps of antigen recognition, proliferation, and differentiation into effector subsets [primarily T helper 1 (T_H1) and T_H17] in the draining lymph node (DLN), egress from lymph nodes (LN) and homing into nonlymphoid tissue [central nervous system (CNS)], and modulation of disease progression by the suppressive functions of T_{reg} cells, leading to disease remission (*24*). The EAE model allowed us to comprehensively investigate the role of Piezo1 channels in transgenic mice with genetic deletion of Piezo1 in T cells and to dissect potential roles in CD4$^+$ T cell homing, motility, priming, and differentiation into effector and T_{reg} cell subsets. In addition, these T cell functions depend critically on TCR-mediated Ca^{2+} signaling via store-operated Ca^{2+} entry (SOCE) through Orai1 channels (*25*). Because Piezo1

[1]Department of Physiology and Biophysics, University of California, Irvine, CA 92697-4561, USA. [2]Sue and Bill Gross Stem Cell Research Center, University of California, Irvine, CA 92697, USA. [3]Howard Hughes Medical Institute, Department of Neuroscience, The Scripps Research Institute, La Jolla, CA 92037, USA. [4]Vertex Pharmaceuticals, 3215 Merryfield Row, San Diego, CA 92121, USA. [5]Department of Neurobiology and Behavior, University of California, Irvine, CA 92697, USA. [6]Department of Biomedical Engineering, University of California, Irvine, CA 92697, USA. [7]Center for Complex Systems Biology, University of California, Irvine, CA 92697, USA. [8]Institute for Immunology, University of California, Irvine, CA 92697, USA.
*Corresponding author. Email: mcahalan@uci.edu
†These authors contributed equally to this work.

channels are also Ca^{2+} permeable, we assessed their role in TCR Ca^{2+} signaling using transgenic mice expressing the genetically encoded Ca^{2+} indicator Salsa6f (*26*), with or without concomitant deletion of Piezo1 in T cells, enabling us to assess both Piezo1 channel function and SOCE. We find that deletion of Piezo1 in T cells diminishes the severity of EAE, which we attribute to its selective role in regulating the induced expansion of T_{reg} cells, while sparing T cell homing, motility, TCR priming, and effector T cell functions.

RESULTS

T lymphocytes express functional Piezo1 channels

We have previously shown that $CD4^+$ T cells exhibit Ca^{2+} elevations in response to Yoda1, a selective Piezo1 agonist (*27*), raising the possibility that Ca^{2+}-permeable Piezo1 channels are functionally expressed in T cells (*26*). To visualize the distribution of Piezo1 on the T cell plasma membrane (PM), $CD4^+$ T cells from *Piezo1*$^{P1\text{-}tdT}$ transgenic mice, in which endogenous Piezo1 channels are tagged with the fluorescent protein tdTomato at the C terminus (*12*), were plated on anti-CD3 and anti-CD28 antibody-coated coverslips and imaged by total internal reflectance fluorescence (TIRF) microscopy. Tagged Piezo1 channels with a punctate localization pattern in the PM were visible throughout the cell footprint, similar to their PM distribution in neural stem cells (Fig. 1A) (*28*).

To study the role of Piezo1 in $CD4^+$ T cell function, we crossed *Piezo1*$^{fl/fl}$ mice with *Cd4-Cre* mice to generate conditional knockout *Cd4-Piezo1*$^{-/-}$ mice with T cell–specific deletion of Piezo1 (Fig. 1B, top); knockdown of Piezo1 mRNA transcripts was confirmed by reverse transcription quantitative polymerase chain reaction (RT-qPCR) (Fig. 1B, bottom). As expected, addition of Yoda1 increased cytosolic Ca^{2+} levels in $CD4^+$ T cells from *Cd4-Cre* control mice, consistent with expression of functional Piezo1 channels in the PM. Yoda1-induced Ca^{2+} responses were absent in $CD4^+$ T cells from *Cd4-Piezo1*$^{-/-}$ mice, confirming functional knockout of Piezo1 (Fig. 1, C and D). Yoda1 responses were also lacking in $CD8^+$ T cells from *Cd4-Piezo1*$^{-/-}$ mice, consistent with Cre activity at the double positive ($CD4^+$ $CD8^+$) stage of thymic development leading to Piezo1 deletion in both $CD4^+$ and $CD8^+$ T cells (Fig. 1E). Finally, we performed patch-clamp studies in $CD4^+$ T cells either expressing or lacking Piezo1. In wild-type (WT) $CD4^+$ T cells, local application of Yoda1 activated a nonselective cationic current, which was reversed upon Yoda1 washout and blocked by Gd^{3+} (Fig. 1, F and G). The nearly linear current-voltage relationship with a reversal potential around 0 mV is characteristic of nonselective Piezo1 channels (*29*). In contrast, Yoda1-induced currents were completely absent in T cells lacking Piezo1 (Fig. 1, F to H), confirming that Piezo1 channels are functional in $CD4^+$ T cells.

To determine whether Piezo1 plays a role in T cell development, we analyzed primary and secondary lymphoid organs and found that the sizes of LN, spleen, and thymus were similar in *Cd4-Cre* and *Cd4-Piezo1*$^{-/-}$ mice, as were the total numbers of splenic $CD4^+$ and $CD8^+$ T cells and the relative abundances of T cell subsets (Fig. 1, I to K). These results suggest that deletion of Piezo1 in T cells does not alter thymic selection or the homeostatic distribution of T cells among the secondary lymphoid organs. In summary, Piezo1 channels are functionally expressed in T cells and are dispensable for T cell development in the thymus, at least beyond the double-positive stage.

$CD4^+$ T cell homing and interstitial motility are conserved in the absence of Piezo1

Piezo1 has been shown to modulate motility in a variety of cell types including endothelial cells, metastatic breast cancer cells, and gastric cancer cells (*14*, *30*, *31*). Normal seeding of *Piezo1*$^{-/-}$ $CD4^+$ T cells into secondary lymphoid organs prompted us to more broadly evaluate the functional importance of Piezo1 in $CD4^+$ T cell homing and in shaping motility patterns within the LN, processes that underlie optimal antigen search and immune response. To delineate the role of Piezo1 in homing, we separately labeled equal numbers of $CD4^+$ T cells expressing or lacking Piezo1 with different cell tracker dyes, and coadoptively transferred the cells into WT recipient mice (Fig. 2A). Similar numbers of input cells were recovered from the subcutaneous DLNs of the recipient mice after 18 hours, suggesting that Piezo1 is not essential for $CD4^+$ T cell homing to the LN (Fig. 2, B and C). To evaluate whether Piezo1 regulates interstitial motility of T cells, we tracked cell motility characteristics in LN by two-photon microscopy (Fig. 2D, Video S1). Both control and *Piezo1*$^{-/-}$ $CD4^+$ T cells showed typical stop-and-go motility; plots of cellular displacement, which depict an overlay of cell tracks from a fixed origin, also revealed similar patterns (Fig. 2, E and F). Instantaneous three-dimensional (3D) velocities and the related mean track speeds were marginally reduced in *Piezo1*$^{-/-}$ T cells (Fig. 2, G and H). Measures of track straightness—meandering index and directionality ratio—were indistinguishable, indicating that T cells lacking Piezo1 exhibit the same turning behavior as control cells (Fig. 2, I and J). Mean square displacement (MSD) plots and average motility coefficients confirmed similar random walk behavior for the two cell types (Fig. 2, K and L). In summary, deletion of Piezo1 does not affect homing or interstitial motility of $CD4^+$ T cells in the LN.

Deletion of Piezo1 in T cells ameliorates autoimmune neuroinflammation

To investigate the role of Piezo1 in $CD4^+$ T cell–mediated immune responses in vivo, we studied disease progression in a murine model of EAE (*24*, *26*, *32*, *33*). Active EAE was induced in WT controls and *Cd4-Piezo1*$^{-/-}$ mice by immunization with myelin oligodendrocyte glycoprotein peptide fragment 35-55 ($MOG_{35–55}$) peptide emulsified in complete Freund's adjuvant (CFA) (Fig. 3A). In both WT controls and *Cd4-Piezo1*$^{-/-}$ mice, the clinical scores progressively increased after the same initial onset at day 10, reaching a peak around day 16. However, average disease scores were significantly lower in *Cd4-Piezo1*$^{-/-}$ mice (Fig. 3B), due to more rapid remission during 15 to 25 days postimmunization (DPI). The attenuation of disease severity in *Cd4-Piezo1*$^{-/-}$ mice was confirmed by area under the curve analysis of the clinical scores (Fig. 3C).

We analyzed cells from DLN at 10 DPI to gain insight into the abundance of T_H1 and T_H17 effector T cell subsets, which drive the inflammatory damage seen in EAE (*34*, *35*). LN and spleen were comparable in size in control and *Cd4-Piezo1*$^{-/-}$ mice, suggesting no major differences in overall cell numbers (Fig. 3D). The relative numbers of T_H1 cells were, however, significantly reduced in the DLN of *Cd4-Piezo1*$^{-/-}$ mice, although T_H17 cell numbers were similar (Fig. 3, E to H). To specifically assess the effects of Piezo1 expression on the encephalitogenic potential of effector T cells in vivo, we used an adoptive-transfer model of EAE (AT-EAE) and compared the ability of $MOG_{35–55}$-expanded control *Cd4-Cre* and *Cd4-Piezo1*$^{-/-}$ cells to elicit neuroinflammation in recipient

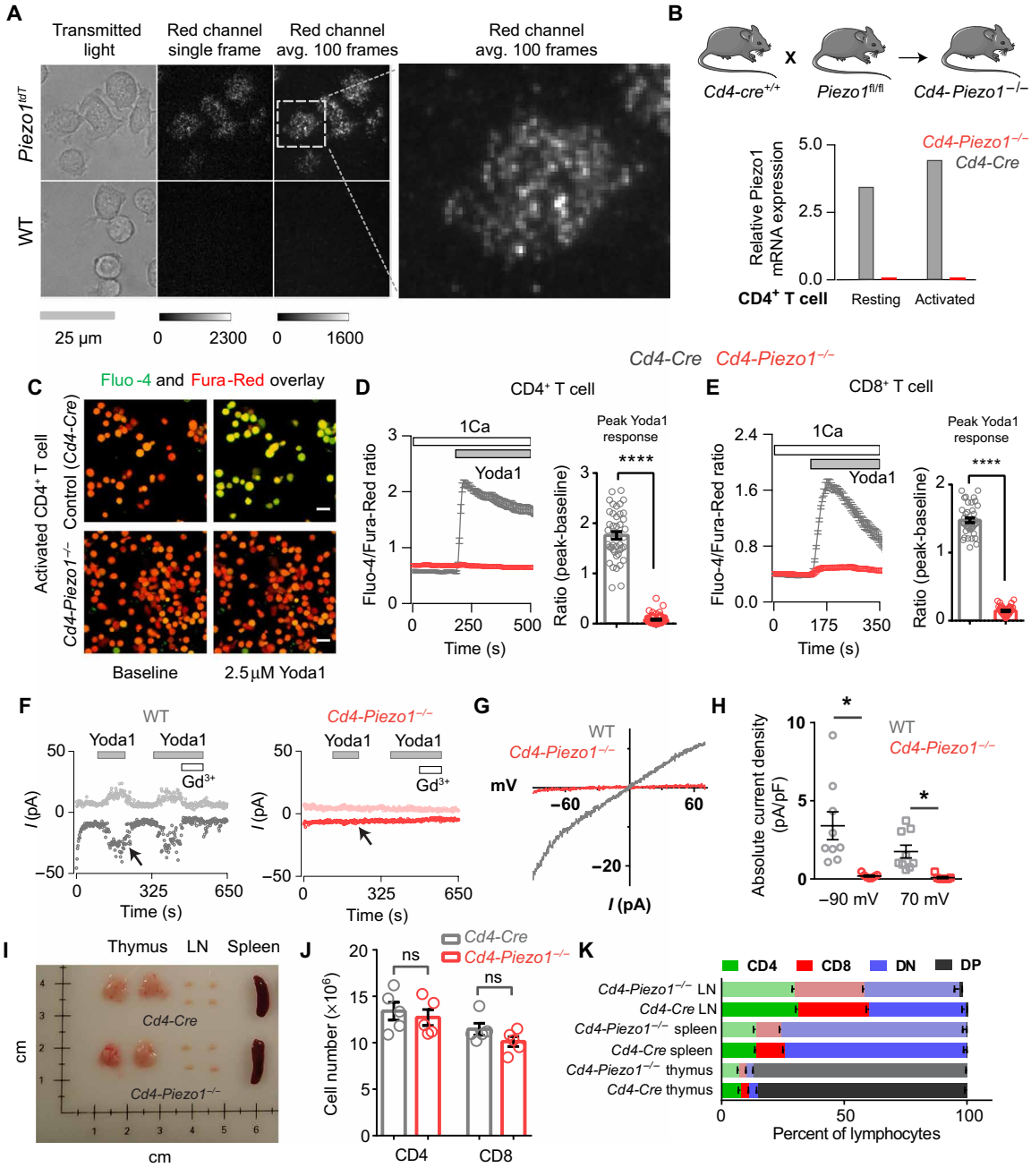

Fig. 1. Functional expression of Piezo1 channels in T cells and their role in T cell development. (**A**) Bright-field and TIRF images (single and averaged over 100 frames) of activated CD4$^+$ T cell from *Piezo1*$^{P1\text{-}tdT}$ and control WT mice. A magnified, averaged TIRF image shows the distribution of Piezo1-tdTomato at the PM. (**B**) Experimental strategy to delete expression of Piezo1 in CD4$^+$ cells (top). RT-PCR confirmation of Piezo1 knockout in naïve and activated CD4$^+$ T cells (bottom). Data pooled from cells isolated from two mice in each group. (**C**) Representative merged green (Fluo-4) and red (Fura-Red) images showing CD4$^+$ T cells before and after Yoda1 addition. Scale bars, 20 µm. (**D** and **E**) Ca^{2+} responses evoked by Yoda1 (2.5 µM) in *Cd4-Cre* (gray) and *Cd4-Piezo1*$^{-/-}$ (red) CD4$^+$ and CD8$^+$ T cells (****$P < 0.0001$, Mann-Whitney test, $n = 54$ to 63 CD4$^+$ T cells and 40 to 43 CD8$^+$ T cells, two independent experiments). (**F**) Yoda1-activated (10 µM) current in WT control and *Cd4-Piezo1*$^{-/-}$ T cells recorded at −90 mV (dark) and +70 mV (light). Bars indicate Yoda1 (10 µM) and Gd^{3+} (10 µM) application. (**G**) Corresponding current-voltage relationships at times indicated in (F). (**H**) Current densities of Yoda1-evoked currents in WT (gray; $n = 9$ cells) and *Cd4-Piezo1*$^{-/-}$ (red; $n = 7$) T cells; *$P < 0.01$, one-way analysis of variance (ANOVA) with multiple comparisons. (**I**) Thymus, LN, and spleen from *Cd4-Cre* and *Cd4-Piezo1*$^{-/-}$ mice. Photo credit: Shiva Othy, UCI. (**J**) Total numbers of CD4$^+$ and CD8$^+$ T cells in the spleens of *Cd4-Cre* and *Cd4-Piezo1*$^{-/-}$ mice ($n = 5$ mice). (**K**) Relative percentages of CD4$^+$; CD8$^+$; CD4$^-$ CD8$^-$ (DN); CD4$^+$ CD8$^+$ (DP) cells in the LN, spleen, and thymus; DN in the LN and spleen broadly refer to non–T cells ($n = 5$ mice; error bars represent SEM).

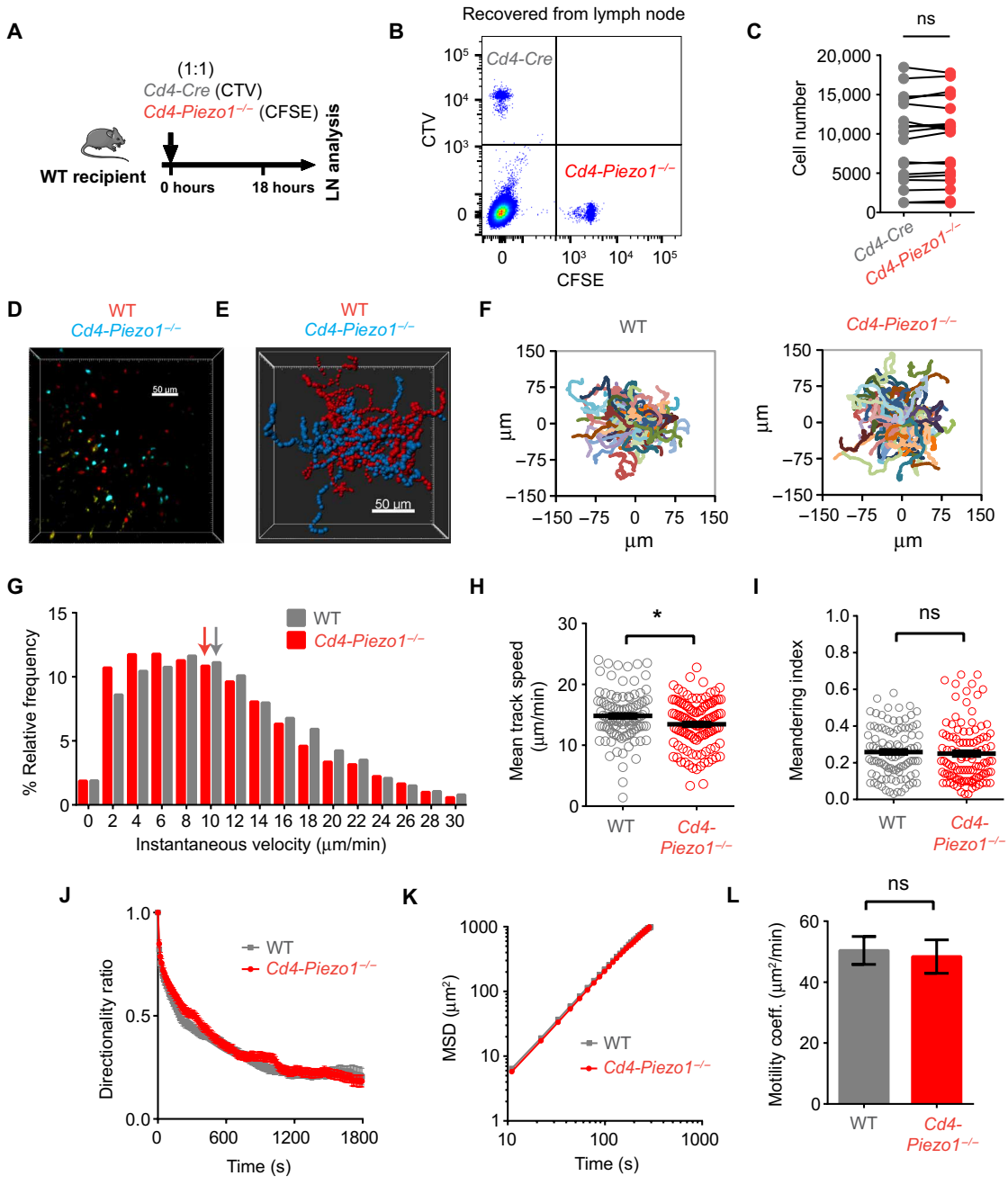

Fig. 2. Homing and motility of *Piezo1*$^{-/-}$ CD4$^+$ T cells in LN following adoptive transfer. (**A**) Experimental design for LN homing assay. (**B**) Dot plots showing recovered cells at 18 hours after injection. (**C**) Numbers of cells recovered from LN ($P = 0.43$, paired t test, $n = 18$ LN, three mice). (**D**) Maximum intensity projection image showing WT control and *Piezo1*$^{-/-}$ CD4$^+$ cells in LN. Scale bar, 50 µm. See movie S1. (**E**) Corresponding migration of WT and *Piezo1*$^{-/-}$ CD4$^+$ cells over 20 min. Spots are superimposed with their starting coordinates normalized to the origin. Scale bar, 50 µm. (**F**) Superimposed cell tracks with origins normalized to the starting coordinates. Cells tracked for >20 min ($n \geq 99$ tracks, three imaging fields). (**G**) Frequency distribution of instantaneous velocities; arrows indicate medians, 10.2 and 9.5 µm/min, for WT and *Piezo1*$^{-/-}$ CD4$^+$ cells, respectively ($n \geq 10{,}089$ cell positions, three imaging fields). (**H**) Mean track speeds (*$P = 0.04$). (**I**) Meandering index (track displacement/track length) for last time point in each track. (**J**) Directionality ratio (displacement/distance) over elapsed time for control and *Piezo1*$^{-/-}$ CD4$^+$ cells ($n = 165$ time points). (**K**) MSD versus time. (**L**) Measured 3D motility coefficients ($M = \text{MSD}/6t$). [For (H), (I), and (L), Mann-Whitney test was used to compare P value, $n \geq 99$ tracks, three imaging fields].

WT mice (Fig. 3I and fig. S1). Transfer of $MOG_{35–55}$-expanded effector cells (including T_H1 and T_H17) from *Cd4-Piezo1*$^{-/-}$ donors into WT recipients induced disease onset with a slight delay compared to control cells, but peak disease scores, remission time course, and overall disease severity were similar (Fig. 3, J and K). On the basis of these observations, we infer that the encephalitogenic potential of T cells is similar in the absence of Piezo1.

To assess whether Piezo1 is required for antigen-specific expansion of CD4$^+$ T cells, we performed a $MOG_{35–55}$ antigen recall assay on cells isolated from EAE-induced control and *Cd4-Piezo1*$^{-/-}$ mice

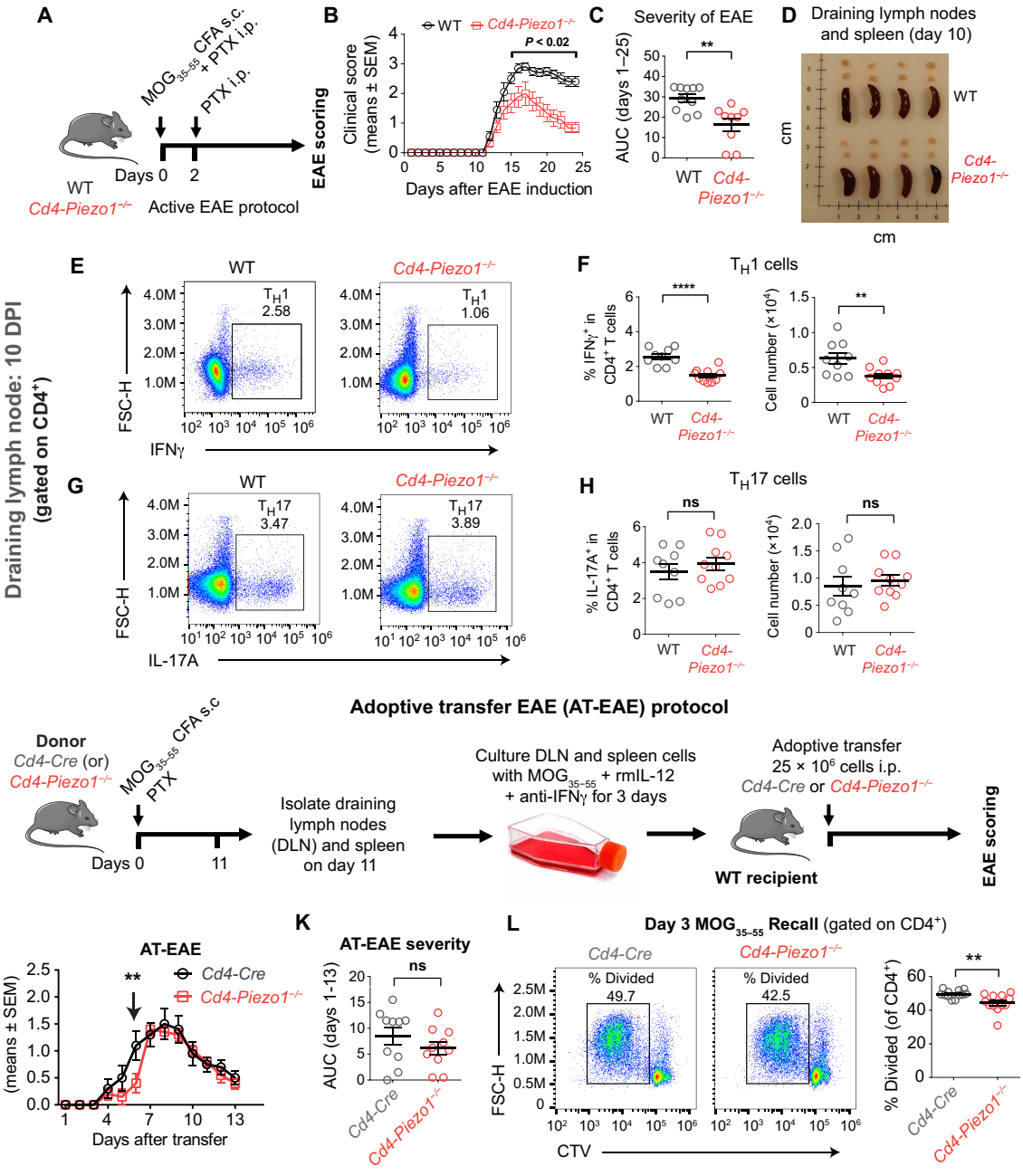

Fig. 3. Effect of T cell–specific Piezo1 deletion in EAE. (**A**) Induction of active EAE. s.c., subcutaneously; i.p., intraperitoneally; PTX, pertussis toxin. (**B**) Mean clinical scores showing progression of disease ($P = 0.0218$ for days 15 to 25, $n = 9$ to 10 mice per group). (**C**) Severity of EAE calculated as area under the curve (AUC) of the clinical score (**$P < 0.01$). (**D**) LN and spleen at 10 DPI. Photo credit: Shiva Othy, UCI. (**E** to **H**) T_H1 and T_H17 cells in the DLN at 10 DPI after treatment with phorbol 12-myristate 13-acetate (PMA), ionomycin, and GolgiStop. (E) Dot plots showing interferon-γ (IFNγ)$^+$ CD4$^+$ cells. (F) Percentages and numbers of T_H1 cells. (G and H) Dot plots and numbers of interleukin-17A (IL-17A)$^+$ T_H17 cells [for (F) and (H), **$P < 0.01$, ****$P < 0.0001$]. (**I**) Induction of AT-EAE. (**J**) Progression of AT-EAE in WT recipients injected with indicated donor cells (**$P < 0.01$ at 6 DPI, $n = 10$ mice per group). (**K**) Severity of EAE calculated as in (C). (**L**) Antigen recall assay: proliferation in cells from DLN at 11 DPI and expanded with $MOG_{35–55}$ peptide for 72 hours in vitro. Dot plots showing CellTrace Violet (CTV) dilution (left) and percent divided cells (right) among CD4$^+$ cells (**$P < 0.01$, $n = 12$ samples pooled from five mice). FSC-H, forward scatter height.

at 11 DPI. Restimulation in vitro with $MOG_{35–55}$ peptide led to a small but significant decrease in the expansion of CD4$^+$ T cells from *Cd4-Piezo1*$^{-/-}$ mice (Fig. 3L). Together with the reduced T_H1 cells in the DLN with the active EAE model (cf. Fig. 3F), this result can be interpreted to mean that Piezo1 deletion either directly reduces effector T cell polarization and proliferation or enhances T_{reg} cell function, which then indirectly mediates the reduction of effector T cell numbers and disease severity. To address these possibilities, we sought to understand at the single-cell level, the effect of Piezo1 deletion on TCR-mediated Ca^{2+} signaling, proliferation, and differentiation in CD4$^+$ T cells, events that are required for EAE onset and progression.

TCR-evoked Ca^{2+} signaling in $CD4^+$ T cells is unaffected by Piezo1 deletion

To study the effects of Piezo1 in T cell Ca^{2+} signaling, we generated transgenic mice that express the Ca^{2+} probe Salsa6f in T cells that either express or lack Piezo1 (Fig. 4A). Addition of Yoda1 selectively increased cytosolic Ca^{2+} in Salsa6f$^+$ control but not in *Piezo1*$^{-/-}$ $CD4^+$ T cells, confirming functional deletion of Piezo1 (Fig. 4, B and C) and consistent with Fig. 1D. However, deletion of Piezo1 did not affect SOCE, a critical pathway for Ca^{2+} influx in T cells, as evidenced by similar rate of Ca^{2+} entry in *Piezo1*$^{-/-}$ and control T cells following endoplasmic reticulum (ER) store depletion with thapsigargin (Fig. 4D). To determine whether Piezo1 affects cytosolic Ca^{2+} levels downstream of TCR activation, we compared the patterns of Ca^{2+} signals in control and *Piezo1*$^{-/-}$ $CD4^+$ T cells incubated with anti-CD3– and anti-CD28–coated beads. Fluctuations in single-cell Ca^{2+} levels were readily observed in both cell types but only in those cells that were in contact with beads (Fig. 4, E and F). Statistical analysis of single-cell Ca^{2+} patterns revealed that the average baseline, peak amplitude, and cumulative Ca^{2+} levels over time were similar in T cells expressing or lacking Piezo1 (Fig. 4G). Analogous results were obtained in T cells in which TCR activation was achieved in solution by preincubation with biotin anti-CD3 and cross-linking with streptavidin (Fig. 4, H and I), as well as in $CD4^+$ T cells stimulated by plate-bound anti-CD3 and anti-CD28 (fig. S2). Together, cross-linking of TCR revealed that Piezo1 does not modulate TCR-mediated Ca^{2+} signaling under several differing mechanical contexts.

Piezo1 does not affect $CD4^+$ T cell proliferation but selectively restrains T_{reg} cells

Results from the antigen recall assay during EAE (Fig. 3, F and L, and fig. S1) suggested a possible defect in the proliferative or polarization capacity of Piezo1-deficient $CD4^+$ T cells. We compared the proliferation of purified $CD4^+$ T cells from control *Cd4-Cre* and *Cd4-Piezo1*$^{-/-}$ mice by dye dilution following activation with anti-CD3– and anti-CD28–coated beads in vitro and found no differences in their proliferative capacity (Fig. 5, A and B). We next considered the possibility that Piezo1 might play a role in the polarization of helper T cells. Purified $CD4^+$ or naïve ($CD4^+CD44^{low}CD62L^{high}CD25^-$) T cells were stimulated in the presence of polarizing cytokines to generate T_H1, T_H17, and T_{reg} cell subsets in vitro (fig. S3A). *Piezo1*$^{-/-}$ $CD4^+$ T cells and naïve T cells polarized into T_H1 and T_H17 inflammatory subsets to the same extent as control T cells, as measured by expression of the signature inflammatory markers interferon-γ (IFNγ) and interleukin-17 (IL-17), respectively (Fig. 5, C to F). Together, Piezo1 does not play a role in either $CD4^+$ T cell proliferation or effector T cell (T_H1 and T_H17) polarization.

In contrast, the population of all *Piezo1*$^{-/-}$ $CD4^+$ T cells, but not naïve T cells, showed an increased percentage of forkhead transcription factor Foxp3 expressing (Foxp3$^+$) T_{reg} cells in the presence of transforming growth factor–β (TGFβ) and IL-2 (Fig. 5, G and H). The presence of $CD4^+$ $CD25^+$ T_{reg} cells was a prerequisite for this expansion (Fig. 5I), and IL-2 alone was insufficient (Fig. 5J). Given the critical importance of T_{reg} cells in suppressing autoreactive effector T cells and in driving recovery and remission during EAE (*24*), we focused on effects of Piezo1 in T_{reg} cell function. To elucidate the mechanism by which Piezo1 favors T_{reg} expansion, we first considered the possibility that Ca^{2+} signaling might be altered in *Piezo1*$^{-/-}$ T cells under T_{reg}-polarizing conditions. After confirming Piezo1 deletion in *Cd4-Salsa6f-Piezo1*$^{-/-}$ T_{reg} cells based on the lack of Yoda1 response (fig. S3B), we found similar SOCE and TCR-evoked Ca^{2+} responses as in control cells (fig. S3, C and D). Because TGFβ signaling is critical for T_{reg} cells (*36*), we next considered the possibility that effects of Piezo1 on T_{reg} polarization might be exerted through TGFβ signaling instead. To address this, we examined the phosphorylation of SMAD2/3, which is activated immediately downstream of TGFβ receptors (*37*, *38*), and found that SMAD2/3 phosphorylation was significantly increased in $CD4^+$ T cells lacking Piezo1 (Fig. 5, K and L). Autocrine TGFβ signaling is also implicated in T_H17 cell biology (*39*); accordingly, polarized cells from the spleen and LN showed a higher percentage of T_H17 cells (fig. S4). In summary, our in vitro data show that, while not required for T cell priming and differentiation into proinflammatory $CD4^+$ subsets, Piezo1 modulates TGFβ signaling and restrains T_{reg} cells.

Piezo1 deletion enhances T_{reg} cells in vivo and attenuates EAE

We then asked whether deletion of Piezo1 might lead to a similar expansion of T_{reg} cells in vivo in the context of EAE. Analysis of DLN from WT and *Cd4-Piezo1*$^{-/-}$ mice 10 days after EAE induction revealed a greater abundance of Foxp3$^+$ T_{reg} cells in *Cd4-Piezo1*$^{-/-}$ mice (Fig. 6, A and B). To further assess the T_{reg} population as the disease progressed, we analyzed cells from the spleen and spinal cord of EAE-induced mice at 24 DPI. Although the total numbers of lymphocytes in the spinal cord were similar (Fig. 6C), the fraction of T_{reg} cells was significantly higher in both the spinal cord and spleen of *Cd4-Piezo1*$^{-/-}$ mice (Fig. 6D). These differences were more pronounced among Ki67$^+$ proliferating cells following restimulation with $MOG_{35–55}$ peptide in vitro (Fig. 6E), consistent with expansion of T_{reg} cells. In contrast, under homeostatic conditions, there were no significant differences in the abundance of Foxp3$^+$ T_{reg} cells in the thymus, spleen, and LN from *Cd4-Piezo1*$^{-/-}$ and *Cd4-Cre* control mice (Fig. 6F). Together with the absence of visible inflammation in the mucosa, these findings suggest that Piezo1 does not affect homeostatic T_{reg} development.

We next evaluated the functional capacity of $CD4^+$ $CD25^+$ T_{reg} cells isolated from WT or *Cd4-Piezo1*$^{-/-}$ mice. *Piezo1*$^{-/-}$ T_{reg} cells displayed TCR-triggered Ca^{2+} responses similar to control T_{reg} cells, arguing against any effects of Piezo1 on downstream TCR signaling, similar to what we find in activated T cells (fig. S5, A and B; cf. Fig. 4G). We then performed an in vitro T_{reg} suppression assay to directly compare the inhibitory effects of control and *Piezo1*$^{-/-}$ T_{reg} cells on the proliferation of $CD4^+$ $CD25^-$ conventional T (T_{conv}) cells. T_{conv} cell proliferation was reduced to the same extent in the presence of T_{reg} cells either expressing or lacking Piezo1 (Fig. 6G), suggesting that T_{reg} cells deficient in Piezo1 are not functionally different in their suppressive capacity. Collectively, these results suggest that genetic deletion of Piezo1 favors T_{reg} cell expansion during EAE, leading to a shift in helper T cell balance toward T_{reg} cells in vivo.

To confirm the T_{reg}-specific role of Piezo1 during EAE, we crossed *Piezo1*$^{fl/fl}$ mice with *Foxp3*$^{eGFP\text{-}Cre\text{-}ERT2}$ to generate *Foxp3*$^{eGFP\text{-}Cre\text{-}ERT2}$ *Piezo1*$^{fl/fl}$ mice in which Piezo1 in Foxp3$^+$ T_{reg} cells can be deleted by injection of tamoxifen (Txn). Yoda1-evoked Ca^{2+} responses in T_{reg} cells from *Foxp3*$^{eGFP\text{-}Cre\text{-}ERT2}$ *Piezo1*$^{fl/fl}$ mice were significantly reduced compared to T_{reg} cells from Txn-treated control *Foxp3*$^{eGFP\text{-}Cre\text{-}ERT2}$ mice (Fig. 7A and fig. S5, C to E), although these cells still retained their capacity to respond normally to ionomycin-induced SOCE,

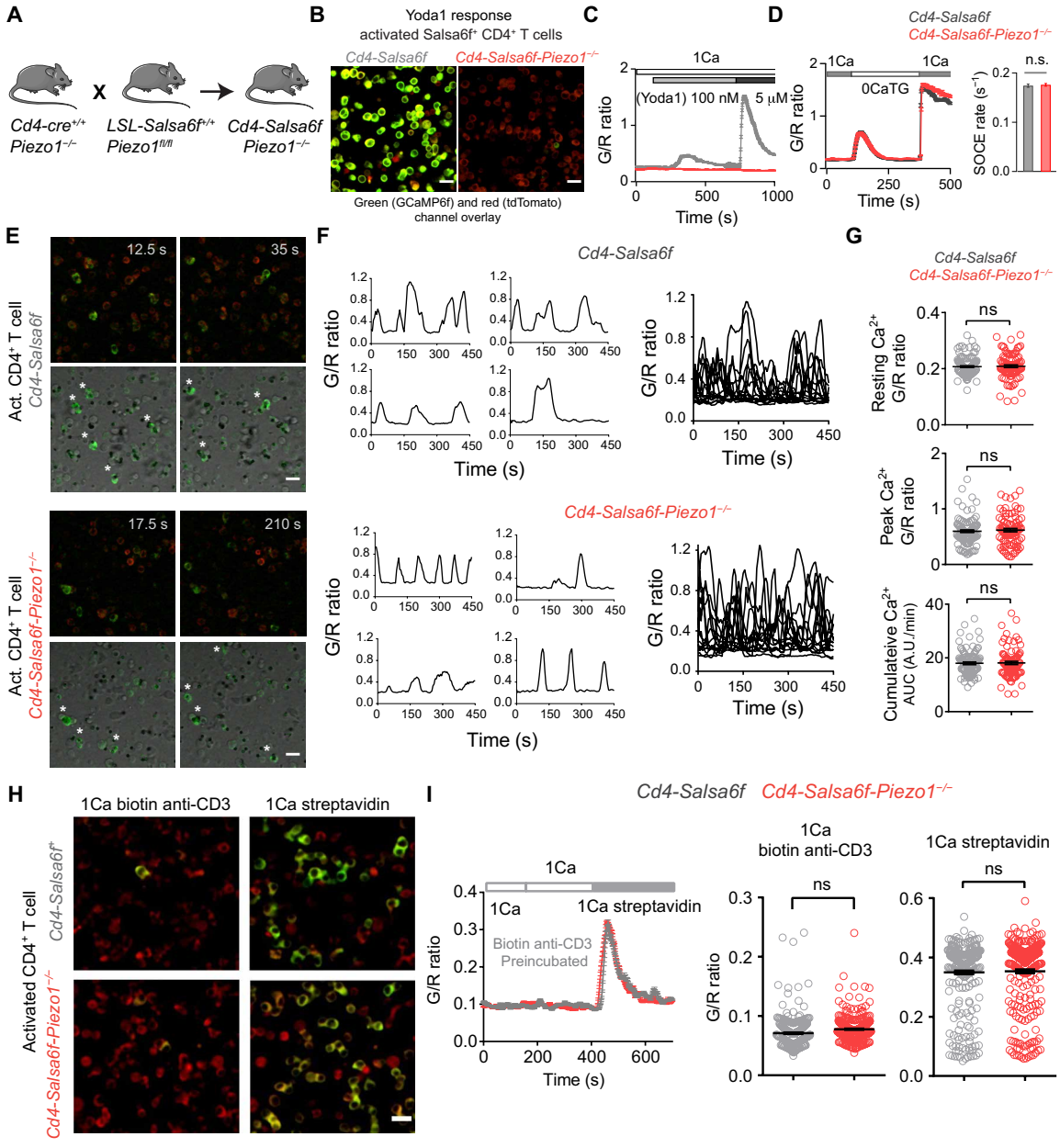

Fig. 4. Role of Piezo1 in regulating TCR-induced Ca^{2+} signals in $CD4^+$ T cells. (**A**) Breeding scheme to simultaneously express Salsa6f and delete Piezo1 in T cells. (**B** and **C**) Ca^{2+} imaging confirming Piezo1 deletion in *Cd4-Salsa6f-Piezo1*$^{-/-}$ T cells. Representative green (GCaMP6f) and red (tdTomato) images 30 s after Yoda1 addition (5 μM) (B) and average single cell Ca^{2+} traces (C) showing changes in GCaMP6f /TdTomato intensity ratio (green/red or G/R ratio) after Yoda1 application (100 nM and 5 μM) in $CD4^+$ T cells from control *Cd4-Salsa6f* and *Cd4-Salsa6f-Piezo1*$^{-/-}$ mice ($n = 81$ to 99 cells, three independent experiments). (**D**) Average Ca^{2+} trace (left) and rate of SOCE (right) in control and *Piezo1*$^{-/-}$ $CD4^+$ T cells (two-tailed unpaired *t* test, $n = 82$ to 83 cells, two independent experiments). (**E** to **G**) Effect of Piezo1 deletion on TCR Ca^{2+} responses to anti-CD3–coated beads. (E) Red (tdTomato) and green (GCamP6f) images (top) and bright-field and green images (bottom) of control and *Piezo1*$^{-/-}$ activated Salsa6f$^+$ $CD4^+$ T cells conjugated with Dynabeads visible as uniform dark spots. (F) Representative single-cell and overlay Ca^{2+} traces of T cells in contact with beads in control (top) and *Piezo1*$^{-/-}$ (bottom) T cells. (G) Analysis of single-cell Ca^{2+} signals in $CD4^+$ T cells with or without Piezo1. Single-cell baseline resting (top), peak (middle), and cumulative Ca^{2+} signals (bottom) (two-tailed Mann-Whitney test, $n = 85$ to 107 cells, two independent experiments). A.U., arbitrary units. (**H** and **I**) Cytosolic Ca^{2+} in T cells pretreated with biotin anti-CD3 and in response to streptavidin cross-linking. (H) Red and green channel images of control (top) and *Piezo1*$^{-/-}$ T cells (bottom) showing Ca^{2+} levels with biotin anti-CD3 before incubation (left) and after streptavidin cross-linking (right). (I) Average of single-cell Ca^{2+} traces (left) and cytosolic Ca^{2+} levels in the presence of biotin anti-CD3 alone and following streptavidin addition ($n = 293$ to 301 cells, pooled from two independent experiments). Scale bars, 20 μm (B, E, and H).

indicating that Txn treatment did not inhibit the ability to generate Ca^{2+} signals. Despite incomplete deletion of Piezo1 in T_{reg} cells, Txn treatment significantly improved clinical scores and reduced disease severity in *Foxp3*$^{eGFP\text{-}Cre\text{-}ERT2}$ *Piezo1*$^{fl/fl}$ mice in the active EAE model (fig. S5F) without affecting the time of onset, pointing to a T_{reg}-specific role for Piezo1 in regulating disease remission in EAE (Fig. 7B). Txn treatment did not affect the number of $Foxp3^+$ T_{reg} cells in the peripheral blood, as expected from normal T_{reg} cell

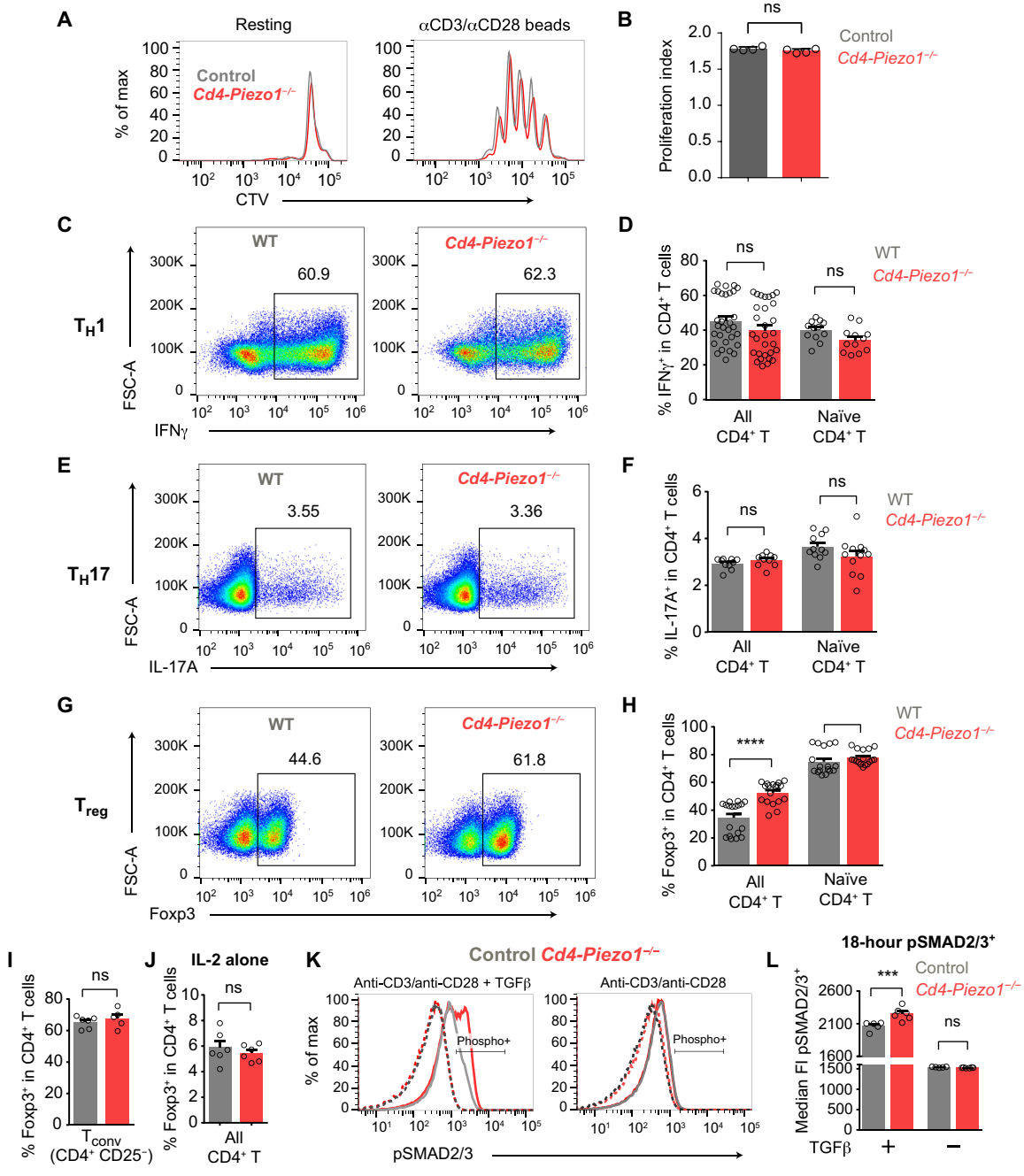

Fig. 5. Effect of Piezo1 deletion on proliferation and polarization of CD4$^+$ T cells in vitro. (**A**) Representative histograms showing CTV dilution in all CD4$^+$ T cells from *Cd4-Cre* (gray) and *Cd4-Piezo1*$^{-/-}$ (red) mice at 72 hours with or without anti-CD3/anti-CD28 Dynabeads (1:1 ratio) and IL-2 (30 U/ml). (**B**) Proliferation index calculated from CTV dilution curves ($n = 4$ samples, two-tailed unpaired t test). (**C** to **H**) Representative flow cytometry plots and percentage of cells after in vitro polarization into T_H1 cells (C and D), T_H17 cells (E and F), and Foxp3$^+$ T_{reg} cells (G and H). Either all CD4$^+$ T cells or naïve (CD4$^+$CD44^{low}CD62L^{high}CD25$^-$) T cells from *Cd4-Cre* and *Cd4-Piezo1*$^{-/-}$ mice were used as starting population. Cells were treated with PMA, ionomycin, and GolgiStop for 4 hours to enable detection of intracellular cytokines. Numbers indicate the percentage of cells in indicated gates. (****$P < 0.0001$, ordinary one-way ANOVA with Sidak's multiple comparisons, data are means ± SEM, $n \geq 9$ samples, two independent experiments). (**I**) Percentage of Foxp3$^+$ cells after in vitro polarization with anti-CD3/anti-CD28 in the presence of IL-2 and TGFβ using CD4$^+$ CD25$^-$ conventional T (T_{conv}) cells as starting population. (**J**) Percentage of Foxp3$^+$ cells after in vitro polarization with anti-CD3/anti-CD28 in the presence of IL-2 alone using all CD4$^+$ cells as starting population. (**K** and **L**) SMAD2/3 phosphorylation determined by antibody staining in CD4$^+$ T cells treated with TGFβ (10 ng/ml) and anti-CD3/anti-CD28 for 18 hours. (**K**) Representative histograms showing levels of pSMAD2/3 in control (gray) and *Cd4-Piezo1*$^{-/-}$ (red) cells, corresponding that dashed lines represent phosphatase-treated controls. (**L**) Median fluorescence intensity of phosphorylated-SMAD2/3$^+$ cells (***$P < 0.001$, ordinary one-way ANOVA with Sidak's multiple comparisons, $n > 5$ samples, pooled from three mice). FSC-A, forward scatter area.

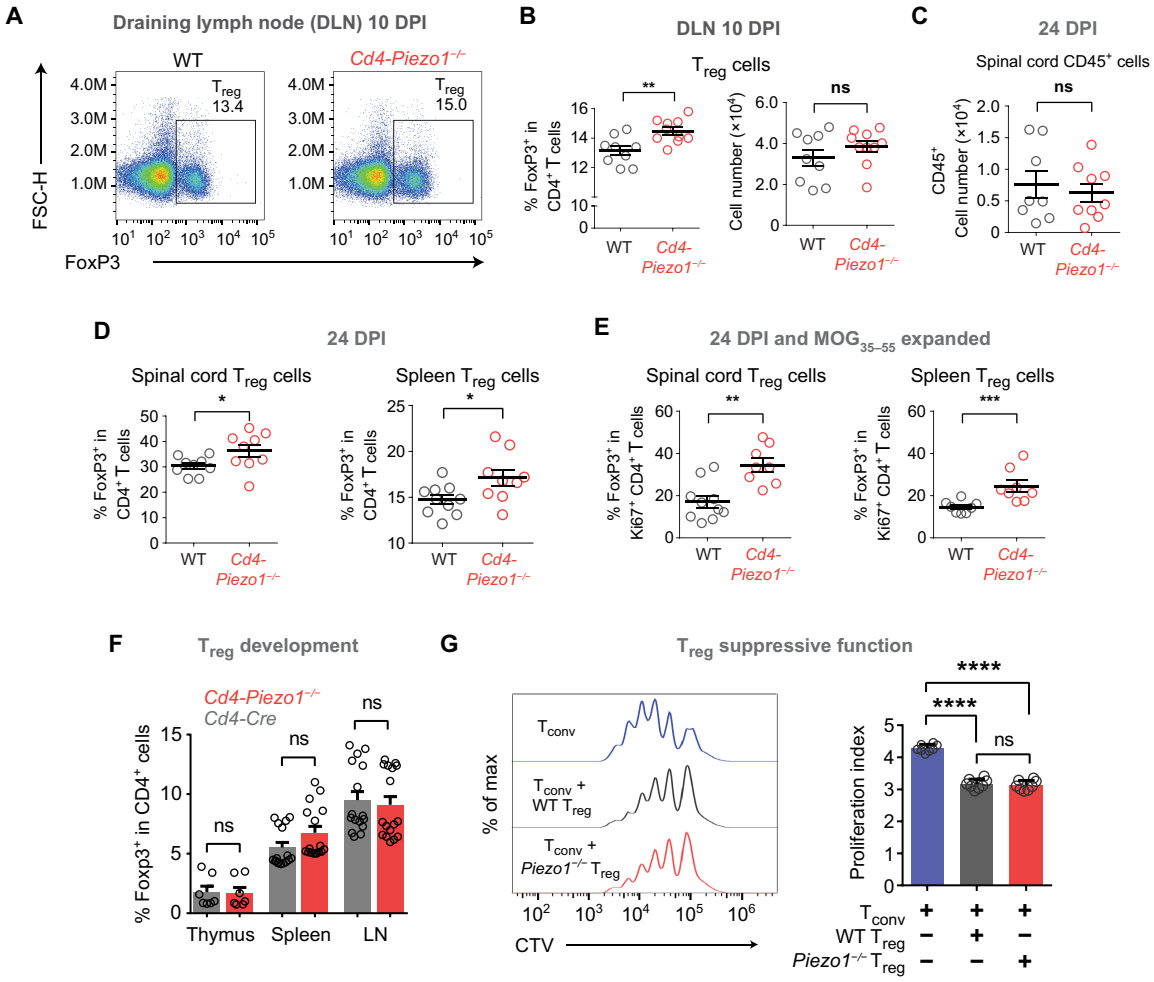

Fig. 6. T cell–specific deletion of Piezo1 enhances T_{reg} cell number in vivo during EAE. (**A** and **B**) Foxp3$^+$ cells in the DLN 10 days after EAE induction. (**A**) Dot plots showing Foxp3$^+$ cells gated on CD4$^+$ cells. (**B**) Summary of percentages and numbers of Foxp3$^+$ cells. (**C**) Numbers of CD45$^+$ cells in the spinal cords of WT and *Cd4-Piezo1*$^{-/-}$ mice 24 DPI. (**D**) Numbers of T_{reg} cells in the spinal cord (left) and spleen (right) 24 DPI. (**E**) Percentage of T_{reg} cells isolated 24 DPI and after 72-hour incubation with $MOG_{35–55}$ peptide. [For (A) to (E), *$P < 0.05$, **$P < 0.01$, and ***$P < 0.001$, two-tailed unpaired *t* test, $n = 9$ WT and 10 *Cd4-Piezo1*$^{-/-}$ mice]. (**F**) Numbers of Foxp3$^+$ CD4$^+$ T cells in the thymus, LN, and spleen of *Cd4-Piezo1*$^{-/-}$ mice and control *Cd4-Cre* mice ($n = 7$ to 16). (**G**) Representative histograms showing CTV dilution (left) and proliferation index (right) of WT CD4$^+$CD25$^-$ T_{conv} cells after 72-hour stimulation with anti-CD3 and anti-CD28–coated Dynabeads alone or in the presence of T_{reg} cells [****$P < 0.0001$, one-way ANOVA with multiple comparisons for (A) and (C), $n = 8$ samples].

numbers under homeostatic conditions in the secondary lymphoid organs of *Cd4-Piezo1*$^{-/-}$ mice, and suggesting that the effects of Piezo1 on T_{reg} cells manifest only after an immune challenge (fig. S5G; cf. Fig. 6F). To further evaluate effects of T_{reg}-specific Piezo1 knockdown, we adoptively transferred $MOG_{35–55}$-expanded WT encephalitogenic cells in to recipient mice with or without inducible deletion of Piezo1 in T_{reg} cells (fig. S5H). Again, we found that T_{reg}-specific knockdown of Piezo1 significantly reduced clinical signs and overall disease severity (Fig. 7C). Correspondingly, these mice also showed greater survival rates than controls (Fig. 7D). Overall, these results further support a model in which Piezo1 limits EAE remission by constraining T_{reg} cells.

DISCUSSION

Our main finding is that deletion of Piezo1 mechanosensitive ion channels in T cells ameliorates disease severity in EAE, an in vivo murine model of multiple sclerosis. Using genetic deletion, we found that Piezo1 is dispensable in CD4$^+$ T cells for thymic development, LN homing, interstitial motility, TCR priming to induce Ca^{2+} signaling, T cell proliferation, effector T_H1 and T_H17 cell polarization, and encephalitogenicity. However, Piezo1 selectively restrains T_{reg} cells, thus limiting their potential to mitigate autoimmune neuroinflammation.

We provide comprehensive evidence to confirm the expression of functional Piezo1 channels in CD4$^+$ T cells: detection of Piezo1 transcripts in CD4$^+$ T cell subsets; the presence of discrete puncta of native Piezo1-tdTomato protein in the PM of CD4$^+$ T cells from Piezo1$^{P1\text{-}tdT}$ mice; elevated cytosolic Ca^{2+} in response to Yoda1, a selective agonist of Piezo1, that is abrogated in T cells lacking Piezo1; and Yoda1-induced currents observed by whole-cell patch recording in WT but not *Piezo1*$^{-/-}$ CD4$^+$ T cells. Despite robust expression, deletion of Piezo1 did not significantly alter the proportion of CD4$^+$ or CD8$^+$ T cells in the thymus, LN, and spleen, indicating

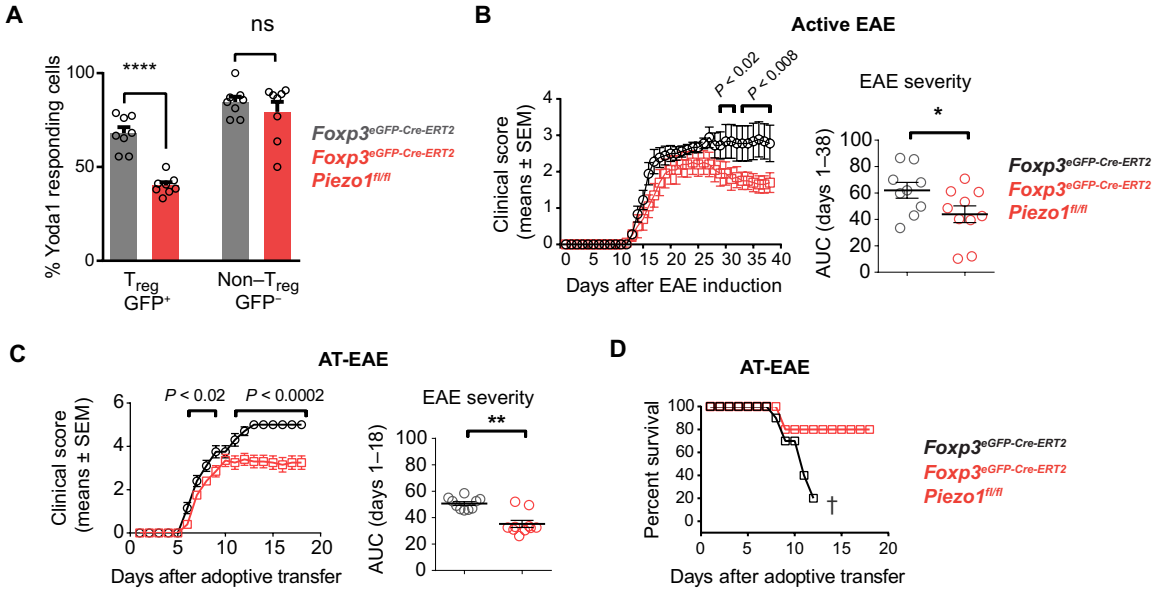

Fig. 7. T_{reg}-specific deletion of Piezo1 ameliorates severity of EAE. (**A**) Confirmation of Txn-induced deletion of Piezo1 in T_{reg} cells by Cal590 Ca^{2+} imaging showing the fraction of green fluorescent protein (GFP)$^+$ T_{reg} cells and GFP$^-$ T_{conv} cells responding to Yoda1 in control (*Foxp3*$^{eGFP\text{-}Cre\text{-}ERT2}$) mice and *Foxp3*$^{eGFP\text{-}Cre\text{-}ERT2}$ *Piezo1*$^{fl/fl}$ mice treated with Txn (****$P < 0.0001$, one-way ANOVA with multiple comparisons, $n = 8$ fields of view, 164 to 184 cells) (**B** to **D**) Effect of T_{reg}-specific *Piezo1* deletion on progression of active and AT-EAE. (B) Clinical scores showing progression of active EAE (left) and disease severity (right) in Txn-treated *Foxp3*$^{eGFP\text{-}Cre\text{-}ERT2}$ *Piezo1*$^{fl/fl}$ mice (red) and *Foxp3*$^{eGFP\text{-}Cre\text{-}ERT2}$ control mice (black). (Left: $P < 0.02$ for 30 DPI and $P < 0.008$ for days 33 to 38 DPI, two-way ANOVA with multiple comparisons; right: *$P < 0.05$, Mann-Whitney test, $n = 9$ to 10 mice). (C) Clinical scores and disease severity in the AT-EAE model. (Left: $P < 0.02$, days 6 to 9 and $P < 0.0002$, days 11 to 18, two-way ANOVA with multiple comparisons; right: **$P < 0.01$, Mann-Whitney test, $n = 10$ mice). (D) Enhanced survival of mice with T_{reg}-specific Piezo1 knockdown ($P = 0.023$, two-way ANOVA, $n = 10$ mice).

that T cell development and the seeding of mature T cells into secondary lymphoid organs occur independently of Piezo1 channels.

We examined the role of Piezo1 in five key T cell functions that operate in sequence during the pathophysiology of EAE: (i) homing to LNs and interstitial motility to search for cognate antigen, (ii) the initial priming of T cells in DLNs, (iii) differentiation of primed T cells into proinflammatory effector T_H1 and T_H17 subsets, (iv) migration of effector T cells into the spinal cord resulting in the onset of symptoms, and (v) T_{reg}-mediated amelioration of EAE. We consider these five events below in sequence. Overall, our results are consistent with involvement of Piezo1 in T_{reg} cell expansion, thus impairing T_{reg} cell–mediated mitigation of neuroinflammation. First, we show that homing and motility characteristics of *Piezo1*$^{-/-}$ CD4$^+$ T cells in the LNs are similar to control T cells. Second, Ca^{2+} signaling induced by TCR engagement was not affected in *Piezo1*$^{-/-}$ CD4$^+$ cells in a variety of contexts: anti-CD3 antibodies that are plate-bound, coated on beads, and in solution. Accordingly, proliferation of *Piezo1*$^{-/-}$ CD4$^+$ T cells in response to TCR cross-linking was also indistinguishable from controls. Third, differentiation of purified CD4$^+$ T or naïve T cells into T_H1 and T_H17 effector cells in vitro also proceeded normally in the absence of Piezo1. Fourth, the total numbers of CD45$^+$ cells in the spinal cord at 24 DPI were similar in control and *Cd4-Piezo1*$^{-/-}$ mice, and the similar peak severity in the AT-EAE model further supports the conclusion that migration of activated effector T lymphocytes to the spinal cord does not require Piezo1. Fifth, the augmentation of Foxp3$^+$ T_{reg} cells from purified CD4$^+$ T cells during in vitro polarization, and the elevated frequencies of T_{reg} cells during EAE in vivo strongly indicate a role for Piezo1 in T_{reg} expansion following immunization. Consistent with this, selective deletion of Piezo1 in T_{reg} cells dampened the course of disease in both active and AT-EAE models.

Because TGFβ signaling is crucial for T_{reg} survival and function (*36*), we examined the TGFβ/SMAD signaling pathway in CD4$^+$ T cells and found that SMAD2/3 phosphorylation is augmented in the absence of Piezo1 channels. While we did not explore how Piezo1 channels might restrain signaling downstream of TGFβ receptor, further mechanistic possibilities are suggested by studies in neural stem cells and renal fibroblasts in which Piezo1 regulates the nuclear-cytosolic localization of Yes-associated protein (YAP) and transcriptional coactivator with PDZ-binding motif (TAZ), depending on the substrate stiffness (*13*, *40*). A recent study implicated YAP in T_{reg} cell suppressive function in a cancer model (*41*), whereas another study showed that TAZ reciprocally regulates T_H17 and T_{reg} differentiation (*42*). Whether Piezo1 plays any role in the YAP/TAZ signaling pathway in T cells remains to be investigated. Enhanced TGFβ signaling may be also due to increased access to active TGFβ itself, because integrin-mediated traction forces are required to release TGFβ from latency (*43*), and T_{reg} cells can activate TGFβ via integrin αvβ8 (*44*). The role of Piezo1 in integrin signaling and force generation in T cells is unknown, and the molecular mechanism by which Piezo1 modulates TGFβ signaling merits further investigation.

We further demonstrate that Piezo1-deficient T_{reg} cells develop normally and suppress proliferation of CD4$^+$ CD25$^-$ T_{conv} cells similar to WT controls. In addition, the absence of visible inflammation in the mucosa and comparable cellularity of lymphoid organs in *Cd4-Piezo1*$^{-/-}$ mice suggest that immune homeostasis functions of T_{reg} cells are intact. However, when multiple cellular components

are challenged during a strong autoimmune response, such as EAE, a role of Piezo1 in T_{reg} cell function is unmasked. The increased T_{reg} population we observed in the secondary lymphoid organs and spinal cord of *Cd4-Piezo1*$^{-/-}$ mice may also explain the slightly reduced proliferation of $CD4^+$ cells in the MOG recall assay and the reduced abundance of T_H1 cells in the DLN at 10 DPI, thus providing a possible cellular mechanism wherein the higher degree of suppression by the expanded T_{reg} population reduces EAE severity. Although the T_H17 population was unaffected in *Cd4-Piezo1*$^{-/-}$ mice during EAE, this might be because T_H17 cell differentiation also relies partially on TGFβ, thus compensating for any ensuing suppression by T_{reg} cells. We observed a higher number of T_H17 cells in two in vitro experimental settings: (i) during ex vivo expansion of donor cells for AT-EAE and (ii) during T_H17 polarization from whole LN and spleen cells.

Time-lapse imaging using Salsa6f, a ratiometric genetically encoded Ca^{2+} indicator, enabled us to monitor cytosolic Ca^{2+} levels as a real-time readout of TCR activation and Yoda1 activation of Piezo1. Deletion of Piezo1 produced little change in (i) TCR-mediated Ca^{2+} signaling in three activation paradigms of TCR cross-linking (plate-bound, bead-based, and streptavidin cross-linked) in vitro, (ii) $CD4^+$ T cell proliferation, and (iii) the peak severity of EAE. These results support our conclusion that Piezo1 channels are not required for the initial events of T cell activation, different from conclusions reported previously that small interfering RNA (siRNA)–mediated knockdown of Piezo1 resulted in a reduction in human T cell activation, measured by Zap70 (zeta chain of T cell receptor associated protein kinase 70) phosphorylation, cell proliferation, and Fluo-3 Ca^{2+} imaging (*45*). Possible reasons for this discrepancy include differences in the specific methods used to knock down Piezo1 (siRNA versus genetic knockout) or differences in the role of Piezo1 in human and mouse T cells.

Ion channels play a crucial role in T cell functions and can be pharmacologically targeted using small-molecule antagonists (*46*, *47*). We have previously shown that Ca^{2+} influx through Orai1 channels regulates LN homing (*48*) and interstitial motility (*49*). Patients with loss-of-function mutations in Piezo1 predominantly suffer from lymphedema and overhydrated RBCs (*18*). However, a previous study demonstrated an in vivo impact of a gain-of-function Piezo1 (R2482H) mutation in T cells that conferred partial protection against cerebral malaria in a mouse model without affecting *Plasmodium berghei* parasite clearance (*17*). Our study demonstrates a protective effect of Piezo1 deletion in T cells during EAE, suggesting that the impact of Piezo1 activity in the same cell type may vary on the basis of the specific context. A combination of both Piezo1 and Piezo2 activity is required for the sensing of blood pressure and mechanosensing in the articular cartilage (*15*, *50*). Whether such a synergistic mechanism operates in T cell functions remains to be explored. Recent studies have focused on the immune regulatory role of Piezo1 in innate cells (*22*, *23*); the present study addresses the role in the adaptive compartment, specifically in CD4 helper T cells. Further investigation of the function of Piezo1 in cytotoxic CD8 T cells and B cells is necessary to fully understand the role of mechanotransduction during adaptive immunity.

T cells, including T_{reg} cells (*24*, *51*), undergo significant deformation as they squeeze through spaces, navigate barriers, and interact with APCs. Therefore, a lack of effect of Piezo1 deletion on $CD4^+$ T cell activation, interstitial motility, homing, and transmigration is unexpected given that Piezo1 activity is evoked by changes in membrane tension (*52*). This raises the intriguing possibility that T cells have additional regulatory mechanisms in place to prevent Piezo1 activation. Perhaps promiscuous activation of Piezo1 whenever T cells deform and change their cell shape would be deleterious for T cell function by giving spurious activation signals and may negatively affect the exquisite ability of the TCR to detect and discriminate antigens. Direct evidence of the specific mechanical context in which Piezo1 channels are activated in T cells is lacking. On the basis of our in vitro and in vivo data, we speculate that substantial changes in membrane tension may be required to activate Piezo1 channels, possibly when T cells are navigating through stiff environments such as solid tumors or healing wounds.

In summary, our study explores the role of Piezo1 in $CD4^+$ T cell function in the context of an autoimmune neuroinflammation model. Our results show that deletion of Piezo1 in T cells attenuates the severity of EAE by selectively enhancing T_{reg} cell expansion. Given the vital importance of T_{reg} cells in the amelioration of EAE, we suggest that inhibition of Piezo1 could be beneficial in treatment of neuroinflammatory disorders.

MATERIALS AND METHODS

Study design

We used transgenic mouse strains with T cell– and T_{reg}-specific Piezo1 deletion in conjunction with the $MOG_{35–55}$ peptide–based model of EAE, immune cell imaging, and functional assays to investigate the role of Piezo1 in $CD4^+$ T cell–mediated autoimmune neuroinflammation. In addition to clinical scoring of mice to quantify disease score, we analyzed the LN, spleen, and spinal cord of EAE mice for effector T_H1 and T_H17 and T_{reg} cell subsets to gain insight into the cellular mechanisms by which Piezo1 might affect EAE induction and progression. Yoda1, a selective Piezo1 chemical agonist, was used in Ca^{2+} imaging and patch-clamp studies to confirm functional expression of Piezo1 in T cells. We used in vitro functional assays that cross-link the TCR to study the role of Piezo1 in signaling processes that prime T cells, including T cell proliferation, differentiation and Ca^{2+} signaling. For the latter, we generated transgenic mice expressing the genetically encoded Ca^{2+} indicator Salsa6f and lacking Piezo1 in T cells. Transgenic mice with Txn-induced deletion of Piezo1 in $Foxp3^+$ T_{reg} cells allowed us to elucidate the involvement of Piezo1 in T_{reg} function in the context of EAE. Experiments were performed in replicates as indicated in the figure legends. No outliers were omitted. Age- and sex-matched *Cd4-Cre* or WT mice were used as controls, but we, otherwise, did not randomize or blind our studies.

Mice

All mice were housed in a clean, specific pathogen-free facility at the University of California, Irvine (UCI). Animal care protocols were reviewed and approved by the Institutional Animal Care and Use Committee of UCI (protocol no. AUP-18-176). Both male and female mice from the C57Bl/6 background were used at 8 to 12 weeks of age. *Cd4-Cre*, *Piezo1*$^{P1\text{-}tdT}$, *Piezo1*$^{fl/fl}$, *Foxp3*$^{EGFP\text{-}cre\text{-}ERT2}$, and C57Bl/6 WT mice were obtained from the Jackson laboratory (stock nos. 017336, 029214, 029213, 016961, and 000664, respectively). We chose *Cd4*-driven *Cre* expression because *Lck*-driven *Cre* is known to negatively affect T cell development (*53*, *54*). *Cd4-Cre* mice were crossed with *Piezo1*$^{fl/fl}$ mice to generate *Cd4-Cre Piezo1*$^{fl/fl}$ mice. We term these as *Cd4-Piezo1*$^{-/-}$ mice. R26 LoxP-flanked STOP

(Lox-STOP-Lox or LSL) cassette–Salsa6f calcium reporter mice (*LSL-Salsa6f*) were crossed to *Cd4-Cre* to obtain *Cd4-Salsa6f* mice that transgenically express the Salsa6f reporter in T cells as described before (*26*). *Cd4-Piezo1*$^{-/-}$ mice were crossed with an intermediate strain *LSL-Salsa6f*$^{+/+}$ *Piezo1*$^{fl/fl}$ to generate *Cd4-Cre Salsa6f*$^{+/-}$ *Piezo1*$^{fl/fl}$ mice that selectively express Salsa6f and lack Piezo1 in T cells. We term these as *Cd4-Salsa6f-Piezo1*$^{-/-}$ mice. *Foxp3*$^{eGFP\text{-}Cre\text{-}ERT2}$ mice were bred to *Piezo1*$^{fl/fl}$ to generate *Foxp3*$^{eGFP\text{-}Cre\text{-}ERT2}$ *Piezo1*$^{fl/fl}$ mice in which Piezo1 can be deleted specifically in T_{reg} cells by injecting Txn. We selected *Foxp3*$^{eGFP\text{-}Cre\text{-}ERT2}$ instead of the commonly used *Foxp3*$^{YFP\text{-}Cre}$ to avoid promiscuous Cre activity in the latter (*55*).

EAE induction and T_{reg}-specific deletion of Piezo1

Active EAE was induced in mice by immunization with $MOG_{35–55}$ peptide (1 mg/ml) (MEVGWYRSPFSRVVHLYRNGK) emulsified in CFA supplemented with heat-killed *Mycobacterium tuberculosis* H37Ra (5 mg/ml). One hundred microliters of emulsion (EK-0111, Hooke Laboratories, Lawrence, MA) was injected subcutaneously at two sites over the flank region. In addition, 150 ng of pertussis toxin (PTX) (List Biological Laboratories, Campbell, CA) was injected intraperitoneally on the day of immunization and 48 hours later, as described previously (*24*, *56*). Nutra-Gel wet food (#S4798, Bio-Serv) was provided on the floor of the cage, along with long sipper bottles to facilitate feeding after the onset of EAE. To induce AT-EAE, *Cd4-Cre* and *Cd4-Piezo1*$^{-/-}$ donor mice were first actively immunized with $MOG_{35–55}$ peptide and a single dose of pertussis toxin as described above. Eleven days later, cells were isolated from the inguinal DLN and spleen and were activated in vitro with $MOG_{35–55}$ peptide (20 μg/ml) in the presence of recombinant mouse IL-12 (rmIL-12; 20 ng/ml) (p70, containing both p40 and p35 subunits) and anti-IFNγ (10 μg/ml) (clone XMG1.2, BioLegend; to protect MOG-responsive cells from activation-induced cell death) for 72 hours. A total of 25×10^6 donor cells were injected (intraperitoneally) into each WT recipient mice as described previously (*57*). Pertussis toxin was not used for AT-EAE to maintain integrity of the blood-brain barrier in the recipient mice. To delete Piezo1 in T_{reg} cells, *Foxp3*$^{eGFP\text{-}Cre\text{-}ERT2}$ *Piezo1*$^{fl/fl}$ mice were injected with Txn (100 mg/kg) for five successive days (*58*). *Foxp3*$^{eGFP\text{-}Cre\text{-}ERT2}$ mice treated with Txn were used as controls. To maintain Piezo1 deletion during EAE progression, mice were treated with another round of Txn 14 to 18 DPI. To induce AT-EAE, *Foxp3*$^{eGFP\text{-}Cre\text{-}ERT2}$ *Piezo1*$^{fl/fl}$ and control *Foxp3*$^{eGFP\text{-}Cre\text{-}ERT2}$ recipient mice were first treated with Txn for five successive days. $MOG_{35–55}$-expanded cells from WT donor mice were prepared as described above for AT-EAE and injected into recipient mice 4 days after the final Txn treatment. Clinical scores for EAE were assessed daily according to the following scale: 0, no signs; 0.5, partially limp tail; 1, limp tail; 1.5, limp tail and hind leg inhibition; 2, hind limb paresis; 2.5, one hind limb paralysis; 3, both hind limb paralysis; 3.5, hind limb paralysis and weakness in forelimbs; 4, tetraplegia; and 5, moribund or euthanized because of severe paralysis (scored ≥3.5 for two consecutive days).

Isolation of single cells from tissues

Thymus, LN, and spleen were dissected from *Cd4-Cre* and *Cd4-Piezo1*$^{-/-}$ mice. Tissues were homogenized on top of a 70-μm cell strainer to obtain single-cell suspension. Spinal cords were removed from phosphate-buffered saline (PBS)–perfused mice and mechanically dissociated using a Dounce grinder (#K8853000007, Thermo Fisher Scientific) to obtain single-cell suspensions. Twenty-three percent of Percoll (catalog no. 17089101, GE Life Sciences) density gradient centrifugation at 400*g* without brakes for 25 min at 4°C was used to separate myelin debris from cells. The myelin layer at the interface was removed, and the mononuclear cells in the pellet were collected. Blood collection was performed by submandibular bleeding. RBC lysis was performed using ACK buffer (#A1049201, Thermo Fisher Scientific) for 90 s on ice.

T cell activation for Ca^{2+} measurements and electrophysiology in vitro

All $CD4^+$ or $CD8^+$ T cells were isolated from the spleen and LN of 8- to 12-week-old mice using EasySep negative isolation kits, catalog nos. 19852 and 19853, respectively (STEMCELL Technologies, Cambridge, MA). Purity of isolated T cells was confirmed to be >95% by flow cytometry. Isolated T cells were either used for experiments as "resting" T cells or were plated on activating polystyrene surface in six-well plates (Corning Inc., Corning, NY) coated with plate-bound anti-CD3 (2.5 μg/ml; clone 145-2C11) and anti-CD28 (2.5 μg/ml; clone 37.51) and soluble rmIL-2 (30 U/ml; BioLegend) for 2 to 3 days to obtain "activated" T cells for Ca^{2+} measurements and electrophysiology. Unless otherwise stated, cells were cultured in "T cell culture medium": RPMI 1640 medium with 10% fetal bovine serum (FBS), L-glutamine, nonessential amino acids, sodium pyruvate, β-mercaptoethanol, and penicillin–streptomycin–amphotericin B, as described previously (*26*).

Helper T cell polarization in vitro

All $CD4^+$ T cells or naïve ($CD4^+CD44^{low}CD62L^{high}CD25^-$) T cells were isolated from the spleen and LN of 8- to 12-week-old mice, as described in the previous section. For $CD4^+$ $CD25^-$ T_{conv} cell isolation, $CD4^+$ $CD25^+$ T_{reg} cells were removed from the population of all $CD4^+$ cells by using a CD25-positive selection kit (catalog no. 130-091-072, Miltenyi Biotec; or catalog no. 18783, STEMCELL Technologies). For polarization, isolated cells were stimulated on plate-bound anti-CD3 and anti-CD28 in flat-bottom 96-well plate in absence (T_H0) or in the presence of specific T_H subtype–polarizing cytokines for 3 to 4 days. For T_H1 cells, rmIL-12 (25 ng/ml; BioLegend, San Diego, CA) and anti-mouse IL4 (10 μg/ml; BioLegend). For T_H17 cells, rmTGFβ1 (2.5 ng/ml; Tonbo Biosciences, San Diego, CA), rmIL-6 (50 ng/ml; Tonbo Biosciences), rmIL-23 (25 ng/ml; BioLegend), rmIL-1β (25 ng/ml; BioLegend), and anti-mouse IFNγ (10 μg/ml). For T_{reg} cells, rmTGFβ1 (10 ng/ml) and rmIL-2 (100 U/ml; BioLegend). To activate TCR signaling in the T lymphocyte subpopulation of cells isolated from the spleen and LN, soluble anti-CD3 (100 ng/ml; 145-2C11) antibodies were added to the whole cell suspension in round-bottom 96-well plates under specific T_H subtype-polarizing conditions as stated above for T_H1, T_H17 and Treg cells.

Real-time PCR

$CD4^+$ T cells were isolated, washed with PBS, and centrifuged to generate cell pellets that were snap-frozen in liquid nitrogen. Total RNA was isolated using an Aurum RNA isolation kit (Bio-Rad Laboratories). Complementary DNA was synthesized with SuperScript IV Reverse Transcriptase (Invitrogen) following the manufacturer's instructions. qRT-PCR was performed with QuantStudio 7 Flex System using TaqMan Universal PCR Master Mix and probe-based gene-expression assays: Piezo1, Mm01241549; 18 s, Mm03928990; glyceraldehyde-3-phosphate dehydrogenase, Mm99999915; and Tbp (TATA-box binding protein), Mm01277042 (Applied Biosystems).

Data were collected using Applied Biosystems QuantStudio Real-Time PCR software and were analyzed by the comparative cycle threshold (C_T) method using 18*S* to normalize C_T values.

TIRF microscopy

TIRF imaging was performed on an Olympus IX81 microscope with a home-built TIRF illumination system, Olympus 60× 1.45 numerical aperture (NA) PlanApoN TIRF objective, Photometrics DualView2 image splitter, Photometrics Evolve 512 electron-multiplying charge-coupled device (EMCCD) camera, 488-nm argon ion laser (6 mW nominal), and a 561-nm solid state laser (50 mW nominal) as described (*59*). Sixteen-bit images were acquired using the EMCCD camera operated at 100 ms per frame at an electron-multiplying gain of 130. Average illumination intensities were calculated at 2 W/cm^2 (488-nm laser) and 1 W/cm^2 (561-nm laser). Two color images were acquired simultaneously from T cells illuminated with both lasers; the red channel was used to image Piezo1-TdTomato, while the green channel was used to detect the presence of cell autofluorescence. Using the 60× TIRF objective, a pixel corresponded to a 267-nm square. Cells were imaged at room temperature in Ringer's solution with 1 mM Ca^{2+}. Image processing was performed using ImageJ (*60*).

Electrophysiology

Whole-cell recordings were performed as described (*59*) . Briefly, the patch pipette resistance was 3 to 5 megohms; pipette capacitance was completely compensated; series resistance was 80% compensated; and seal resistances were >10 gigaohms. Membrane potentials were corrected for the liquid junction potential (−13.8 mV) between the pipette and bath solutions. Experiments were performed at room temperature. After establishing whole-cell recording, the membrane potential was held at 0 mV, and voltage ramps from −90 to +70 mV alternating with 220-ms pulses to −80 mV were applied every 2 s. All *I-V* curves are averages of five traces and are leak-subtracted. Leak was recorded after 10 μM $GdCl_3$ was applied to block Piezo1 current and fitted with a fifth-order polynomial function. Solutions were applied through a gravity-driven local perfusion system; complete local solution exchange was achieved within ~2 s. The composition of external solution was 126 mM NaCl, 4.5 mM KCl, 2 mM $CaCl_2$, 1 mM $MgCl_2$, 10 mM Hepes, 10 mM glucose (pH 7.4), and an osmolality of 278 mosm. The internal solution contained 115mM CsAsp, 3 mM Cs_4EGTA, 1 mM $CaCl_2$, 12 mMMg-gluconate$_2$, 4 mM Na_2 adenosine 5′-triphosphate, 0.4 mM Na_2 guanosine 5′-triphosphate, 15 mM Hepes (pH 7.2), and an osmolality of 272 mosm. Yoda1 was added to the external solution at final concentration 10 μM just before the experiment. Data were analyzed using Pulse (HEKA Elektronik), Microsoft Excel (Microsoft), and Origin (OriginLab Corp.).

Intracellular Ca^{2+} measurements

Cell preparation and Ca^{2+} imaging protocols

$CD4^+$ T cells expressing the genetically encoded Ca^{2+} indicator Salsa6f were used to measure intracellular Ca^{2+} levels. Ratiometric imaging using Fluo-4 and Fura-Red dyes was used to image Ca^{2+} signals in T cells lacking Salsa6f probe. In T cells expressing *Foxp3*$^{eGFP\text{-}Cre\text{-}ERT2}$ allele, Cal590 dye was used to measure changes in cytosolic Ca^{2+}. Cells were loaded either with 3 μM Fluo-4 AM and 3 μM Fura-Red AM (Molecular Probes) or 3 μM Cal590-AM (AAT Bioquest) in the presence of an equal volume of pluronic acid F-127 (Molecular Probes) for 30 min at 37°C. Cells were washed three times, resuspended in T cell medium, and kept at 37°C. T cells were plated on poly-L-lysine (>300,000 molecular weight, 1 mg/ml in water; Sigma-Aldrich)–coated glass-bottom dishes (35 mm, no. 1.5 thickness, MatTek Corporation) for 15 min and imaged to monitor Ca^{2+} responses to Yoda1 (100 nM to 5 μM) and SOCE in response to thapsigargin (2 μM)–mediated store release. Cells were imaged in 1 mM Ca^{2+} Ringer solution containing 155 mM NaCl, 4.5 mM KCl, 1 mM $CaCl_2$, 0.5 mM $MgCl_2$, 10 mM glucose, and 10 mM Hepes (pH adjusted to 7.4 with NaOH). ER Ca^{2+} stores were depleted in Ca^{2+}-free Ringer solution containing 155 mM NaCl, 4.5 mM KCl, 1.5 mM $MgCl_2$, 10 mM glucose, 1 mM EGTA, and 10 mM Hepes (pH 7.4). To determine Ca^{2+} responses downstream of TCR activation, Salsa6f-expressing 2-day activated $CD4^+$ T cells, day 0 $CD4^+$ $CD25^+$ T_{reg} cells, or 3-day polarized T_{reg} cells were plated on anti-CD3 and anti-CD28 (1 to 2 μg/ml each)–coated 35-mm glass-bottom dishes. For streptavidin cross-linking, cells were preincubated with biotin anti-CD3 (2 μg/ml) for 30 min, washed, and plated on poly-L-lysine–coated coverslips and treated with streptavidin (2 μg/ml) in 1 mM Ca^{2+} Ringers' buffer during imaging. For bead-based activation, Salsa6f-expressing cells were mixed with Dynabeads at 1:1 ratio and plated on collagen-coated coverslips for imaging. Cells that were contact with beads through the duration of imaging (450 s) were analyzed.

Laser scanning confocal microscopy

Cells were imaged on an Olympus FV3000 confocal laser scanning inverted microscope equipped with high-speed resonance scanner, IX3-ZDC2 Z drift compensator, 40× silicone oil objective (NA 1.25), and a Tokai Hit stage top incubation chamber (STXG) to maintain cells at 37°C. To visualize Salsa6f, 488- and 561-nm diode lasers were used for sequential excitation of GCaMP6f (0.3% laser power, 450-V channel voltage, and 494- to 544-nm detector width) and TdTomato (0.05% laser power, 450-V channel voltage, and 580- to 680-nm detector width), respectively. Fluo-4 and Fura-Red were both excited using a 488-nm diode laser (0.07% laser power, 500-V channel voltage, and 494- to 544-nm detector width for Fluo-4; 0.07% laser power, 550-V channel voltage, and 580- to 680-nm detector for Fura-Red). Two high-sensitivity cooled GaAsP photomultiplier tubes (PMTs) were used for detection in the green and red channels, respectively. Image stacks of X = 318.2 μm and Y = 318.2 μm (pixel size, 0.6215 μm by 0.6215 μm) were sequentially acquired at 2- to 3-s intervals using Olympus FV3000 software. Time-lapse videos were time-averaged over three frames to generate a rolling average.

Image analysis

Videos were exported to ImageJ, converted to tiff files, background-subtracted, and single-cell analysis was performed by drawing regions of interest (ROIs) around individual cells in the field. Average intensities in the green and red channels were calculated for each ROI at each time point. GCaMP6f/TdTomato [green/red (G/R) ratio] and Fluo-4/Fura-Red ratio was then obtained to further generate traces showing single-cell and average changes in cytosolic Ca^{2+} over time.

In vitro proliferation

All $CD4^+$ T cells or $CD4^+$ $CD25^-$ T_{conv} cells were labeled with CellTrace Violet (CTV; Thermo Fisher Scientific) and cocultured with anti-CD3– and anti-CD28–coated Dynabeads (Thermo Fisher Scientific) at 1:1 ratio in a round-bottom 96-well plate at 37°C and

5% CO_2 in the dark for 72 hours. For MOG antigen recall assay, cells were isolated from the DLN and spleen from EAE-induced control (*Cd4-Cre*) and *Cd4-Piezo1*$^{-/-}$ mice at 11 DPI, loaded with CTV, expanded in vitro using $MOG_{35–55}$ peptide (20 μg/ml), but without rmIL-12 and anti-IFNγ in round-bottom 96-well plate at 37°C and 5% CO_2 in the dark for 72 hours. Cells were stained for CD4 surface marker and analyzed for CTV dye dilution by flow cytometry. "Proliferation index" was calculated as total number of divisions divided by the number of cells that went into division using FlowJo (*51*).

Flow cytometry

To detect intracellular cytokines, cells were stimulated in with phorbol 12-myristate 13-acetate (PMA), ionomycin, and monensin (GolgiStop, BD Biosciences) for 4 hours at 37°C in T cell culture medium. Cells were first labeled with Ghost Dye Red 780 (Tonbo Biosciences) in PBS for 20 min to eliminate dead cells from analysis. Staining was performed at 4°C after Fc receptors were masked using blocking buffer: 1× PBS/10% fetal bovine serum/unlabeled anti-mouse CD16/32 (1 μg/ml). Anti-CD4 (clone RM4-5), anti-CD8 (clone 53-6.7), anti-CD25 (clone 7D4), and anti-CD45 (clone 30-F11) antibodies were used to label cell surface makers. Cells were washed, fixed, and permeabilized using Foxp3 staining buffer set (Thermo Fisher Scientific). The following antibodies were used to detect intracellular markers: anti–IL-17A (clone TC11-18H10.1), anti-IFNγ (clone XMG1.2), anti-Foxp3 (clone FJK16s), and anti-Ki67 (clone SolA15). Green fluorescent protein (GFP) expressed from the active Foxp3$^{eGFP\text{-}Cre\text{-}ERT2}$ allele was used together with CD4 surface staining to identify Foxp3$^+$ T_{reg} cells in the blood. AccuCheck Counting Beads (PCB100, Thermo Fisher Scientific) were used to estimate cell numbers per sample. Data were acquired using NovoCyte Quanteon (ACEA Biosciences) or BD Fortessa X20 (BD Biosciences) flow cytometers. Fluorescence intensity was plotted against forward scatter area or height (FSC-A or FSC-H), and analyzed using FlowJo analysis software (FlowJo LLC, Ashland, Oregon).

pSMAD2/3 phosphorylation assay

CD4$^+$ T cells were serum-starved for 2 hours, plated on 48-well plates coated with anti-CD3 and anti-CD28 (2.5 μg/ml each) in X-VIVO 15 serum-free medium (Lonza), and incubated with or without TGFβ (10 ng/ml) for 18 hours in the presence of rmIL-2 (30 U/ml). Cells were fixed in 1× BD Phosflow Lyse/Fix Buffer (catalog no. 558049; 10 min at 37°C) and permeabilized in BD Phosflow Perm Buffer III (catalog no. 558050; 30 min on ice). To generate phosphatase-treated controls, 50% of permeabilized cells from each condition were separately incubated with lambda protein phosphatase (8000 U/ml) in 1× NEBuffer containing 1 mM $MnCl_2$ (catalog no. P0753S, New England Biolabs; 30 min at 30°C). Cells were stained with BD Phosflow Alexa Fluor 647 anti-SMAD2 (pS465/pS467)/SMAD3 (pS423/pS425) monoclonal antibody (clone O72-670) and anti–CD4–fluorescein isothiocyanate antibodies. Phosphatase-treated controls were used to exclude the background and gate for phosphorylated SMAD2/3$^+$ cells.

T cell homing and motility in the LN

Labeling and adoptive transfer of T cells

To compare homing and motility characteristics, CD4$^+$ T cells were labeled with 1.6 μM carboxyfluorescein diacetate succinimidyl ester (CFSE) or 10 μM CTV or 10 μM CellTrace Yellow (CTY) for 15 min at 37°C in RPMI 1640 medium without serum. Cells were washed two times with RPMI 1640 containing 10% FBS to remove excess dye and were adoptively transferred into WT recipients at 1:1 ratio. A total of 2 to 3 million cells were injected into recipient mice (intravenously, retro-orbital). Eighteen hours later, LNs were isolated and either used to quantify homing by flow cytometry or imaged by two-photon microscopy to study motility characteristics.

Two-photon microscopy

Multidimensional (XYZT) two-photon microscopy was used to image fluorescently labeled lymphocytes in explanted mouse LNs, as described (*28*). LNs were oriented with the cortex side facing the microscope objective (Nikon 25×, CFI75 Apo L, water immersion; NA, 1.1; working distance, 2.0 mm) on an upright microscope. The node was maintained at 37° ± 0.5°C by perfusion with medium (RPMI 1640) bubbled with carbogen (95% O_2/5% CO_2). A custom-built two-photon microscope based on an Olympus BX51 upright microscope frame, fitted with a motorized Z-Deck stage (Prior), with excitation generated by a tunable femtosecond laser (Chameleon Ultra-II or Vision-II, Coherent) set to 800 nm to excite CFSE, CTV, and CTY. Fluorescence emission was split by 484- and 538-nm dichroic mirrors into three nondescanned PMT detectors (#R3896, Hamamatsu) and used to record the CTV or a second-harmonic signal generated from collagen in blue, CFSE signal in green, and CTY signal in red. For tracking adoptively transferred T cells, 3D image stacks of $x = 350$ μm, $y = 350$ μm, and $z = 52$ μm (voxel size, 0.64 μm by 0.64 μm by 4 μm) were sequentially acquired at 11-s intervals using image acquisition software Slidebook (Intelligent Imaging Innovations) as described previously (*49*). This volume collection was repeated for up to 40 min to create a 4D dataset.

T cell motility analysis

Two-photon–derived videos (XYZT) were processed and analyzed using Imaris software (Bitplane USA, Concord, MA). Median-filtered and histogram-adjusted datasets were used to segment and track cells using Imaris track module. Accuracy of tracking was checked by visually inspecting trajectories in 3D rotated images. *X*, *Y*, and *Z* coordinates of the tracks were used to calculate instantaneous 3D velocity, motility coefficients, MSD, directionality ratio, and mean track speed and to plot tracks as described previously (*49*).

Statistical analysis

GraphPad Prism (version 8.2.0) was used to perform statistical tests and generate *P* values. We used standard designation of *P* values throughout the figures (ns indicates not significant or $P \geq 0.05$; $^*P < 0.05$, $^{**}P < 0.01$, $^{***}P < 0.001$, and $^{****}P < 0.0001$). Data are summarized as bar graphs or scatter plots with bars depicting means ± SEM. Details of number of replicates are provided in the individual figure legends. For comparison between control and Piezo1 deletion groups, a two-tailed nonparametric Mann-Whitney *U* test was used for Ca^{2+} signal analysis, motility analysis, EAE peak disease severity, and T cell differentiation; and a two-tailed unpaired Student *t* test was used for CD4$^+$ T cell subset analysis in the LN, spleen, and spinal cord (T_H1, T_H17, and T_{reg} cells), T cell proliferation, and SMAD2/3 phosphorylation assays. A paired *t* test was used to compare homing of WT and *Piezo1*$^{-/-}$ T cells. For comparison of multiple groups, we used ordinary one-way analysis of variance (ANOVA), followed by either Sidak's or Tukey's multiple comparisons. For calculating significance of EAE clinical scores over several days, we used two-way ANOVA and multiple comparisons using a two-stage linear step-up procedure of Benjamini, Kreiger, and Yekutieli (*61*).

SUPPLEMENTARY MATERIALS

Supplementary material for this article is available at http://advances.sciencemag.org/cgi/content/full/7/28/eabg5859/DC1

View/request a protocol for this paper from *Bio-protocol*.

REFERENCES AND NOTES

1. S. V. Pageon, M. A. Govendir, D. Kempe, M. Biro, Mechanoimmunology: Molecular-scale forces govern immune cell functions. *Mol. Biol. Cell* **29**, 1919–1926 (2018).
2. T. J. Thauland, K. H. Hu, M. A. Bruce, M. J. Butte, Cytoskeletal adaptivity regulates T cell receptor signaling. *Sci. Signal.* **10**, eaah3737 (2017).
3. Y. Liu, N. V. Belkina, C. Park, R. Nambiar, S. M. Loughhead, G. Patino-Lopez, K. Ben-Aissa, J. J. Hao, M. J. Kruhlak, H. Qi, U. H. von Andrian, J. H. Kehrl, M. J. Tyska, S. Shaw, Constitutively active ezrin increases membrane tension, slows migration, and impedes endothelial transmigration of lymphocytes in vivo in mice. *Blood* **119**, 445–453 (2012).
4. S. Faure, L. I. Salazar-Fontana, M. Semichon, V. L. Tybulewicz, G. Bismuth, A. Trautmann, R. N. Germain, J. Delon, ERM proteins regulate cytoskeleton relaxation promoting T cell-APC conjugation. *Nat. Immunol.* **5**, 272–279 (2004).
5. B. Liu, W. Chen, B. D. Evavold, C. Zhu, Accumulation of dynamic catch bonds between TCR and agonist peptide-MHC triggers T cell signaling. *Cell* **157**, 357–368 (2014).
6. Y. Feng, K. N. Brazin, E. Kobayashi, R. J. Mallis, E. L. Reinherz, M. J. Lang, Mechanosensing drives acuity of αβT-cell recognition. *Proc. Natl. Acad. Sci. U.S.A.* **114**, E8204–E8213 (2017).
7. M. Saitakis, S. Dogniaux, C. Goudot, N. Bufi, S. Asnacios, M. Maurin, C. Randriamampita, A. Asnacios, C. Hivroz, Different TCR-induced T lymphocyte responses are potentiated by stiffness with variable sensitivity. *eLife* **6**, e23190 (2017).
8. J. L. Nourse, M. M. Pathak, How cells channel their stress: Interplay between Piezo1 and the cytoskeleton. *Semin. Cell Dev. Biol.* **71**, 3–12 (2017).
9. B. Coste, J. Mathur, M. Schmidt, T. J. Earley, S. Ranade, M. J. Petrus, A. E. Dubin, A. Patapoutian, Piezo1 and Piezo2 are essential components of distinct mechanically activated cation channels. *Science* **330**, 55–60 (2010).
10. B. Coste, B. Xiao, J. S. Santos, R. Syeda, J. Grandl, K. S. Spencer, S. E. Kim, M. Schmidt, J. Mathur, A. E. Dubin, M. Montal, A. Patapoutian, Piezo proteins are pore-forming subunits of mechanically activated channels. *Nature* **483**, 176–181 (2012).
11. S. M. Cahalan, V. Lukacs, S. S. Ranade, S. Chien, M. Bandell, A. Patapoutian, Piezo1 links mechanical forces to red blood cell volume. *eLife* **4**, e07370 (2015).
12. S. S. Ranade, Z. Qiu, S. H. Woo, S. S. Hur, S. E. Murthy, S. M. Cahalan, J. Xu, J. Mathur, M. Bandell, B. Coste, Y. S. Li, S. Chien, A. Patapoutian, Piezo1, a mechanically activated ion channel, is required for vascular development in mice. *Proc. Natl. Acad. Sci. U.S.A.* **111**, 10347–10352 (2014).
13. M. M. Pathak, J. L. Nourse, T. Tran, J. Hwe, J. Arulmoli, D. T. Le, E. Bernardis, L. A. Flanagan, F. Tombola, Stretch-activated ion channel Piezo1 directs lineage choice in human neural stem cells. *Proc. Natl. Acad. Sci. U.S.A.* **111**, 16148–16153 (2014).
14. J. Li, B. Hou, S. Tumova, K. Muraki, A. Bruns, M. J. Ludlow, A. Sedo, A. J. Hyman, L. McKeown, R. S. Young, N. Y. Yuldasheva, Y. Majeed, L. A. Wilson, B. Rode, M. A. Bailey, H. R. Kim, Z. Fu, D. A. Carter, J. Bilton, H. Imrie, P. Ajuh, T. N. Dear, R. M. Cubbon, M. T. Kearney, R. K. Prasad, P. C. Evans, J. F. Ainscough, D. J. Beech, Piezo1 integration of vascular architecture with physiological force. *Nature* **515**, 279–282 (2014).
15. W. Z. Zeng, K. L. Marshall, S. Min, I. Daou, M. W. Chapleau, F. M. Abboud, S. D. Liberles, A. Patapoutian, PIEZOs mediate neuronal sensing of blood pressure and the baroreceptor reflex. *Science* **362**, 464–467 (2018).
16. W. Sun, S. Chi, Y. Li, S. Ling, Y. Tan, Y. Xu, F. Jiang, J. Li, C. Liu, G. Zhong, D. Cao, X. Jin, D. Zhao, X. Gao, Z. Liu, B. Xiao, Y. Li, The mechanosensitive Piezo1 channel is required for bone formation. *eLife* **8**, e47454 (2019).
17. S. Ma, S. Cahalan, G. LaMonte, N. D. Grubaugh, W. Zeng, S. E. Murthy, E. Paytas, R. Gamini, V. Lukacs, T. Whitwam, M. Loud, R. Lohia, L. Berry, S. M. Khan, C. J. Janse, M. Bandell, C. Schmedt, K. Wengelnik, A. I. Su, E. Honore, E. A. Winzeler, K. G. Andersen, A. Patapoutian, Common piezo1 allele in african populations causes RBC dehydration and attenuates plasmodium infection. *Cell* **173**, 443–455.e12 (2018).
18. V. Lukacs, J. Mathur, R. Mao, P. Bayrak-Toydemir, M. Procter, S. M. Cahalan, H. J. Kim, M. Bandell, N. Longo, R. W. Day, D. A. Stevenson, A. Patapoutian, B. L. Krock, Impaired PIEZO1 function in patients with a novel autosomal recessive congenital lymphatic dysplasia. *Nat. Commun.* **6**, 8329 (2015).
19. R. Zarychanski, V. P. Schulz, B. L. Houston, Y. Maksimova, D. S. Houston, B. Smith, J. Rinehart, P. G. Gallagher, Mutations in the mechanotransduction protein PIEZO1 are associated with hereditary xerocytosis. *Blood* **120**, 1908–1915 (2012).
20. S. Ma, A. E. Dubin, Y. Zhang, S. A. R. Mousavi, Y. Wang, A. M. Coombs, M. Loud, I. Andolfo, A. Patapoutian, A role of PIEZO1 in iron metabolism in mice and humans. *Cell* **184**, 969–982.e13 (2021).
21. H. Atcha, A. Jairaman, J. R. Holt, V. S. Meli, R. R. Nagalla, P. K. Veerasubramanian, K. T. Brumm, H. E. Lim, S. Othy, M. D. Cahalan, M. M. Pathak, W. F. Liu, Mechanically activated ion channel Piezo1 modulates macrophage polarization and stiffness sensing. *Nat. Commun.* **12**, 3256 (2021).
22. A. G. Solis, P. Bielecki, H. R. Steach, L. Sharma, C. C. D. Harman, S. Yun, M. R. de Zoete, J. N. Warnock, S. D. F. To, A. G. York, M. Mack, M. A. Schwartz, C. S. Dela Cruz, N. W. Palm, R. Jackson, R. A. Flavell, Mechanosensation of cyclical force by PIEZO1 is essential for innate immunity. *Nature* **573**, 69–74 (2019).
23. B. Aykut, R. Chen, J. I. Kim, D. Wu, S. A. A. Shadaloey, R. Abengozar, P. Preiss, A. Saxena, S. Pushalkar, J. Leinwand, B. Diskin, W. Wang, G. Werba, M. Berman, S. K. B. Lee, A. Khodadadi-Jamayran, D. Saxena, W. A. Coetzee, G. Miller, Targeting Piezo1 unleashes innate immunity against cancer and infectious disease. *Sci. Immunol.* **5**, eabb5168 (2020).
24. S. Othy, A. Jairaman, J. L. Dynes, T. X. Dong, C. Tune, A. V. Yeromin, A. Zavala, C. Akunwafo, F. Chen, I. Parker, M. D. Cahalan, Regulatory T cells suppress Th17 cell $Ca2^{+}$signaling in the spinal cord during murine autoimmune neuroinflammation. *Proc. Natl. Acad. Sci. U.S.A.* **117**, 20088–20099 (2020).
25. S. Feske, H. Wulff, E. Y. Skolnik, Ion channels in innate and adaptive immunity. *Annu. Rev. Immunol.* **33**, 291–353 (2015).
26. T. X. Dong, S. Othy, A. Jairaman, J. Skupsky, A. Zavala, I. Parker, J. L. Dynes, M. D. Cahalan, T-cell calcium dynamics visualized in a ratiometric tdTomato-GCaMP6f transgenic reporter mouse. *eLife* **6**, e32417 (2017).
27. R. Syeda, J. Xu, A. E. Dubin, B. Coste, J. Mathur, T. Huynh, J. Matzen, J. Lao, D. C. Tully, I. H. Engels, H. M. Petrassi, A. M. Schumacher, M. Montal, M. Bandell, A. Patapoutian, Chemical activation of the mechanotransduction channel Piezo1. *eLife* **4**, e07369 (2015).
28. K. L. Ellefsen, J. R. Holt, A. C. Chang, J. L. Nourse, J. Arulmoli, A. H. Mekhdjian, H. Abuwarda, F. Tombola, L. A. Flanagan, A. R. Dunn, I. Parker, M. M. Pathak, Myosin-II mediated traction forces evoke localized Piezo1-dependent $Ca2^{+}$ flickers. *Commun. Biol.* **2**, 298 (2019).
29. V. Deivasikamani, S. Dhayalan, Y. Abudushalamu, R. Mughal, A. Visnagri, K. Cuthbertson, J. L. Scragg, T. S. Munsey, H. Viswambharan, K. Muraki, R. Foster, A. Sivaprasadarao, M. T. Kearney, D. J. Beech, P. Sukumar, Piezo1 channel activation mimics high glucose as a stimulator of insulin release. *Sci. Rep.* **9**, 16876 (2019).
30. C. Li, S. Rezania, S. Kammerer, A. Sokolowski, T. Devaney, A. Gorischek, S. Jahn, H. Hackl, K. Groschner, C. Windpassinger, E. Malle, T. Bauernhofer, W. Schreibmayer, Piezo1 forms mechanosensitive ion channels in the human MCF-7 breast cancer cell line. *Sci. Rep.* **5**, 8364 (2015).
31. X. N. Yang, Y. P. Lu, J. J. Liu, J. K. Huang, Y. P. Liu, C. X. Xiao, A. Jazag, J. L. Ren, B. Guleng, Piezo1 is as a novel trefoil factor family 1 binding protein that promotes gastric cancer cell mobility in vitro. *Dig. Dis. Sci.* **59**, 1428–1435 (2014).
32. M. Koutrolos, K. Berer, N. Kawakami, H. Wekerle, G. Krishnamoorthy, Treg cells mediate recovery from EAE by controlling effector T cell proliferation and motility in the CNS. *Acta Neuropathol. Commun.* **2**, 163 (2014).
33. M. J. McGeachy, L. A. Stephens, S. M. Anderton, Natural recovery and protection from autoimmune encephalomyelitis: Contribution of $CD4^{+}CD25^{+}$ regulatory cells within the central nervous system. *J. Immunol.* **175**, 3025–3032 (2005).
34. I. M. Stromnes, L. M. Cerretti, D. Liggitt, R. A. Harris, J. M. Goverman, Differential regulation of central nervous system autoimmunity by T(H)1 and T(H)17 cells. *Nat. Med.* **14**, 337–342 (2008).
35. U. Kaufmann, P. J. Shaw, L. Kozhaya, R. Subramanian, K. Gaida, D. Unutmaz, H. J. McBride, S. Feske, Selective ORAI1 inhibition ameliorates autoimmune central nervous system inflammation by suppressing effector but not regulatory T cell function. *J. Immunol.* **196**, 573–585 (2016).
36. J. C. Marie, J. J. Letterio, M. Gavin, A. Y. Rudensky, TGF-β1 maintains suppressor function and Foxp3 expression in $CD4^{+}CD25^{+}$ regulatory T cells. *J. Exp. Med.* **201**, 1061–1067 (2005).
37. T. Takimoto, Y. Wakabayashi, T. Sekiya, N. Inoue, R. Morita, K. Ichiyama, R. Takahashi, M. Asakawa, G. Muto, T. Mori, E. Hasegawa, S. Saika, T. Hara, M. Nomura, A. Yoshimura, Smad2 and Smad3 are redundantly essential for the TGF-β–mediated regulation of regulatory T plasticity and Th1 development. *J. Immunol.* **185**, 842–855 (2010).
38. A. Nakao, T. Imamura, S. Souchelnytskyi, M. Kawabata, A. Ishisaki, E. Oeda, K. Tamaki, J. Hanai, C. H. Heldin, K. Miyazono, P. ten Dijke, TGF-β receptor–mediated signalling through Smad2, Smad3 and Smad4. *EMBO J.* **16**, 5353–5362 (1997).
39. I. Gutcher, M. K. Donkor, Q. Ma, A. Y. Rudensky, R. A. Flavell, M. O. Li, Autocrine transforming growth factor-β1 promotes in vivo Th17 cell differentiation. *Immunity* **34**, 396–408 (2011).
40. S. G. Szeto, M. Narimatsu, M. Lu, X. He, A. M. Sidiqi, M. F. Tolosa, L. Chan, K. De Freitas, J. F. Bialik, S. Majumder, S. Boo, B. Hinz, Q. Dan, A. Advani, R. John, J. L. Wrana, A. Kapus, D. A. Yuen, YAP/TAZ are mechanoregulators of TGF-β-Smad signaling and renal fibrogenesis. *J. Am. Soc. Nephrol.* **27**, 3117–3128 (2016).
41. X. Ni, J. Tao, J. Barbi, Q. Chen, B. V. Park, Z. Li, N. Zhang, A. Lebid, A. Ramaswamy, P. Wei, Y. Zheng, X. Zhang, X. Wu, P. Vignali, C. P. Yang, H. Li, D. Pardoll, L. Lu, D. Pan, F. Pan, YAP is essential for Treg-mediated suppression of antitumor immunity. *Cancer Discov.* **8**, 1026–1043 (2018).

42. J. Geng, S. Yu, H. Zhao, X. Sun, X. Li, P. Wang, X. Xiong, L. Hong, C. Xie, J. Gao, Y. Shi, J. Peng, R. L. Johnson, N. Xiao, L. Lu, J. Han, D. Zhou, L. Chen, The transcriptional coactivator TAZ regulates reciprocal differentiation of TH17 cells and Treg cells. *Nat. Immunol.* **18**, 800–812 (2017).
43. X. Dong, B. Zhao, R. E. Iacob, J. Zhu, A. C. Koksal, C. Lu, J. R. Engen, T. A. Springer, Force interacts with macromolecular structure in activation of TGF-β. *Nature* **542**, 55–59 (2017).
44. J. J. Worthington, A. Kelly, C. Smedley, D. Bauche, S. Campbell, J. C. Marie, M. A. Travis, Integrin αvβ8-mediated TGF-β activation by effector regulatory T cells is essential for suppression of T-cell–mediated inflammation. *Immunity* **42**, 903–915 (2015).
45. C. S. C. Liu, D. Raychaudhuri, B. Paul, Y. Chakrabarty, A. R. Ghosh, O. Rahaman, A. Talukdar, D. Ganguly, Cutting edge: Piezo1 mechanosensors optimize human T cell activation. *J. Immunol.* **200**, 1255–1260 (2018).
46. M. D. Cahalan, K. G. Chandy, The functional network of ion channels in T lymphocytes. *Immunol. Rev.* **231**, 59–87 (2009).
47. M. Vaeth, S. Kahlfuss, S. Feske, CRAC channels and calcium signaling in T cell-mediated immunity. *Trends Immunol.* **41**, 878–901 (2020).
48. M. L. Greenberg, Y. Yu, S. Leverrier, S. L. Zhang, I. Parker, M. D. Cahalan, Orai1 function is essential for T cell homing to lymph nodes. *J. Immunol.* **190**, 3197–3206 (2013).
49. T. X. Dong, S. Othy, M. L. Greenberg, A. Jairaman, C. Akunwafo, S. Leverrier, Y. Yu, I. Parker, J. L. Dynes, M. D. Cahalan, Intermittent $Ca2^{+}$ signals mediated by Orai1 regulate basal T cell motility. *eLife* **6**, e27827 (2017).
50. W. Lee, H. A. Leddy, Y. Chen, S. H. Lee, N. A. Zelenski, A. L. McNulty, J. Wu, K. N. Beicker, J. Coles, S. Zauscher, J. Grandl, F. Sachs, F. Guilak, W. B. Liedtke, Synergy between Piezo1 and Piezo2 channels confers high-strain mechanosensitivity to articular cartilage. *Proc. Natl. Acad. Sci. U.S.A.* **111**, E5114–E5122 (2014).
51. M. P. Matheu, S. Othy, M. L. Greenberg, T. X. Dong, M. Schuijs, K. Deswarte, H. Hammad, B. N. Lambrecht, I. Parker, M. D. Cahalan, Imaging regulatory T cell dynamics and CTLA4-mediated suppression of T cell priming. *Nat. Commun.* **6**, 6219 (2015).
52. A. H. Lewis, J. Grandl, Mechanical sensitivity of Piezo1 ion channels can be tuned by cellular membrane tension. *eLife* **4**, e12088 (2015).
53. J. Shi, H. T. Petrie, Activation kinetics and off-target effects of thymus-initiated cre transgenes. *PLOS ONE* **7**, e46590 (2012).
54. B. Carow, Y. Gao, J. Coquet, M. Reilly, M. E. Rottenberg, lck-driven cre expression alters T cell development in the thymus and the frequencies and functions of peripheral T cell subsets. *J. Immunol.* **197**, 2261–2268 (2016).
55. D. Wu, Q. Huang, P. C. Orban, M. K. Levings, Ectopic germline recombination activity of the widely used Foxp3-YFP-Cre mouse: A case report. *Immunology* **159**, 231–241 (2020).
56. S. Othy, P. Hegde, S. Topcu, M. Sharma, M. S. Maddur, S. Lacroix-Desmazes, J. Bayry, S. V. Kaveri, Intravenous gammaglobulin inhibits encephalitogenic potential of pathogenic T cells and interferes with their trafficking to the central nervous system, implicating sphingosine-1 phosphate receptor 1-mammalian target of rapamycin axis. *J. Immunol.* **190**, 4535–4541 (2013).
57. M. A. Kroenke, T. J. Carlson, A. V. Andjelkovic, B. M. Segal, IL-12- and IL-23-modulated T cells induce distinct types of EAE based on histology, CNS chemokine profile, and response to cytokine inhibition. *J. Exp. Med.* **205**, 1535–1541 (2008).
58. H. M. Jahn, C. V. Kasakow, A. Helfer, J. Michely, A. Verkhratsky, H. H. Maurer, A. Scheller, F. Kirchhoff, Refined protocols of tamoxifen injection for inducible DNA recombination in mouse astroglia. *Sci. Rep.* **8**, 5913 (2018).
59. J. L. Dynes, A. V. Yeromin, M. D. Cahalan, Cell-wide mapping of Orai1 channel activity reveals functional heterogeneity in STIM1-Orai1 puncta. *J. Gen. Physiol.* **152**, e201812239 (2020).
60. C. A. Schneider, W. S. Rasband, K. W. Eliceiri, NIH Image to ImageJ: 25 years of image analysis. *Nat. Methods* **9**, 671–675 (2012).
61. S. M. Tietz, M. Zwahlen, N. Haghayegh Jahromi, P. Baden, I. Lazarevic, G. Enzmann, B. Engelhardt, Refined clinical scoring in comparative EAE studies does not enhance the chance to observe statistically significant differences. *Eur. J. Immunol.* **46**, 2481–2483 (2016).

Acknowledgments: We thank A. Patapoutian for discussion and postdoctoral support of S.M.C. through HHMI. **Funding:** This work was supported by grants R01 NS14609 and R01 AI121945 (to M.D.C.), R37 GM-48071 to (to I.P.), R21 AR072849 (to F.M.), and R01 NS109810 and DP2 AT010376 (to M.M.P.) from the NIH; and by a James H. Gilliam Fellowship for Advanced Study (GT11549) from the Howard Hughes Medical Institute (HHMI) (to J.R.H. and M.M.P.). A.J. and S.O. were supported in part by Hewitt Foundation for Biomedical Research. **Author contributions:** A.J., S.O., and M.D.C. designed the study and wrote the manuscript. A.J. and S.O. performed most of the experiments and acquired and analyzed the data. J.L.D. performed TIRF experiments and analysis. A.V.Y. conducted the patch-clamp recordings. A.Z. monitored the mice and performed injections and cell purifications. J.L.N. and J.R.H. performed RT-PCR experiments. F.M. supervised TGFβ signaling and polarization experiments during revision. M.L.G. and S.M.C. performed some T cell motility experiments. I.P., M.M.P., and M.D.C. supervised the study. **Competing interests:** The authors declare that they have no competing interests. **Data and materials availability:** All data needed to evaluate the conclusions in the paper are present in the paper and/or the Supplementary Materials. Additional data related to this paper may be requested from the authors.

Submitted 14 January 2021
Accepted 24 May 2021
Published 7 July 2021
10.1126/sciadv.abg5859

Citation: A. Jairaman, S. Othy, J. L. Dynes, A. V. Yeromin, A. Zavala, M. L. Greenberg, J. L. Nourse, J. R. Holt, S. M. Cahalan, F. Marangoni, I. Parker, M. M. Pathak, M. D. Cahalan, Piezo1 channels restrain regulatory T cells but are dispensable for effector $CD4^{+}$ T cell responses. *Sci. Adv.* **7**, eabg5859 (2021).